Title: *Wolbachia* endosymbionts manipulate GSC self-renewal and differentiation to reinforce host fertility

Short title: *Wolbachia's* rescue and reinforcement of host fertility

Authors: Shelbi L Russell[1]*, Jennie Ruelas Castillo[2], William T Sullivan[3]

Affiliations:

1. Department of Biomolecular Engineering, University of California Santa Cruz, Santa Cruz, CA, United States
2. Division of Infectious Diseases, Department of Medicine, The Johns Hopkins Hospital, Baltimore, MD, United States
3. Department of Molecular, Cell, and Developmental Biology, University of California Santa Cruz, Santa Cruz, CA, United States

*** corresponding author email: shelbilrussell@gmail.com**

Graphical Abstract:

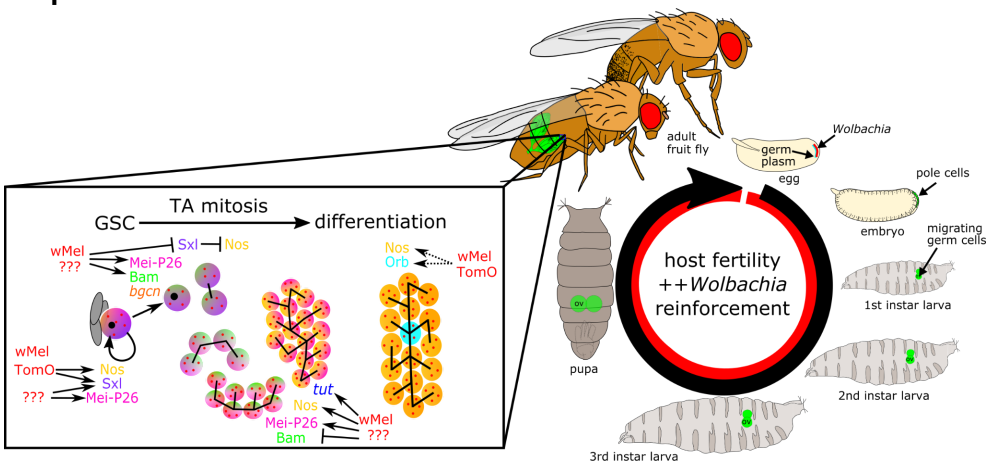

Highlights:

- The wMel strain of *Wolbachia* restores fertility in females and males deficient for the essential translational regulator *meiotic-P26*
- *Mei-P26's* germline maintenance and oocyte cyst differentiation functions are genetically rescued by wMel infection
- Perturbed pMad, Sxl, Bam, and Orb protein expression are mitigated by wMel infection
- wMel infection elevates lifetime egg lay and hatch rates in OreR flies
- Ovary transcriptomes reveal wMel infection restores or offsets changes in gene expression induced by the loss of functional *mei-P26*

Significance Statement:
Wolbachia bacterial symbionts are being harnessed as biological control agents through the use of their costly manipulations to host fertility. Here, we reveal that the *w*Mel strain can have a beneficial impact on fruit fly development in both mutant and wild-type flies. This phenotype is essential to the long-term use of these bacteria for host population control.

Abstract:
The alphaproteobacterium *Wolbachia pipientis* infects arthropod and nematode species worldwide, making it a key target for host biological control. *Wolbachia*-driven host reproductive manipulations, such as cytoplasmic incompatibility (CI), are credited for catapulting these intracellular bacteria to high frequencies in host populations. Positive, perhaps mutualistic, reproductive manipulations also increase infection frequencies, but are not well understood. Here, we identify molecular and cellular mechanisms by which *Wolbachia* influences the molecularly distinct processes of GSC self renewal and differentiation. We demonstrate that *w*Mel infection rescues the fertility of flies lacking the translational regulator *mei-P26*, and is sufficient to sustain infertile homozygous *mei-P26*-knockdown stocks indefinitely. Cytology revealed that *w*Mel mitigates the impact of *mei-P26* loss through restoring proper pMad, Bam, Sxl, and Orb expression. In OreR files with wild-type fertility, *w*Mel infection elevates lifetime egg hatch rates. Exploring these phenotypes through dual-RNAseq experiments revealed that *w*Mel infection rescues and offsets many gene expression changes induced by *mei-P26* loss at the mRNA level. Overall, we show that *w*Mel infection beneficially reinforces host fertility at mRNA, protein, and phenotypic levels, and these mechanisms may promote the emergence of mutualism and the breakdown of host reproductive manipulations.

Introduction:
Endosymbiotic bacteria have evolved diverse strategies for infecting and manipulating host populations [1,2], which are now being leveraged for biological control applications [3]. Many of these bacteria reside within host cells and navigate female host development to colonize offspring, thus linking their fitness to that of their hosts through vertical transmission [4]. Inherited endosymbionts with reproductive manipulator capabilities go a step further by altering host development in ways that rapidly increase the frequency of infected, reproductive females in the host population. Reproductive manipulator strategies include cytoplasmic incompatibility (CI), where infected sperm require rescue by infected eggs, male-killing, feminization, and parthenogenesis [5,6]. These manipulations can be highly effective at driving bacterial symbionts into host populations, regardless of costs to the host individual or population [7].

Despite the success of parasitic reproductive manipulation, natural selection favors symbionts that increase the fertility of infected mothers, even if these variants reduce the efficacy of the parasitic mechanisms that initially drove the infection to high frequency [8]. In associations between arthropods and strains of the alphaproteobacterium *Wolbachia pipientis,* this scenario may be common. For example, measured fecundity in populations of *Drosophila simulans* infected with the wRi strain of *Wolbachia* swung from -20% to +10% across a 20-year span following wRi's CI-mediated sweep across California in the 1980s [9]. This transition from fitness cost to benefit coincided with weakening of CI strength over the same time-frame [10]. Fertility-enhancing mechanisms may be at work in other strains of *Wolbachia* that have reached high infection frequencies in their native hosts, yet do not currently exhibit evidence of parasitic reproductive manipulation [11]. Importantly, these fitness benefits may have also played a role in the early stages of population infection, when infected hosts are at too low of frequencies for CI to be effective [12].

Currently, the *w*Mel strain and its encoded CI mechanism are successfully being used to biologically control non-native hosts [3]. In *Aedes aegypti* mosquitoes, CI causes nearly 100% mortality of offspring born to uninfected mothers [13]. However, in its native host, the fruit fly *Drosophila melanogaster*, *w*Mel exhibits CI that rarely exceeds 50% mortality and is extremely sensitive to paternal age [14–16], as well as grandmother age because titer increases with age [17,18]. Despite weak CI in its native host, *w*Mel is found at moderate to high infection frequencies in populations worldwide [19,20]. Other data suggest that these frequencies may be explained by some emergent beneficial function that increases host fitness [21–25]. The molecular basis for these beneficial functions could be related to the loss of CI efficacy in *D. melanogaster*. Given that *w*Mel's use in non-native hosts relies on strong and efficient CI, it is essential that we learn the basis for its beneficial functions that could ultimately undermine CI function.

Host germline stem cell (GSC) maintenance and differentiation pathways are powerful targets for *Wolbachia*-mediated reproductive manipulation. *Wolbachia* strains have strong affinities for host germline tissues [26,27], positioning them at the right place to manipulate and enhance host fertility. In the strains that form obligate associations with *Brugia* filarial nematodes [28] and *Asobara* wasps [29], *Wolbachia* is required in the germline to prevent premature differentiation and achieve successful oogenesis (reviewed in [30]). In the facultative *w*Mel-*D. melanogaster* association, the *w*Mel strain can partially rescue select loss of function alleles of the essential germline maintenance and differentiation genes *sex lethal (sxl)* and *bag-of-marbles (bam)* in female flies [31–33]. It is known that *w*Mel encodes its own factor, Toxic manipulator of oogenesis (TomO), that partially recapitulates Sxl function in the GSC through derepression and overexpression of the translational repressor Nanos (Nos) [34,35]. However, Nos expression is negatively correlated with Bam expression in the early germarium [36]. Therefore, Bam's function in cyst patterning and differentiation in *w*Mel-infected mutant flies cannot be explained by shared mechanisms with *sxl* rescue or TomO's known functions.

In a previous screen, our lab identified the essential fertility gene *meiotic-P26* (*mei-P26*) as a host factor that influences *w*Mel infection intensity in *D. melanogaster* cell culture, potentially through modulating protein ubiquitination [37]. Mei-P26 is a Trim-NHL protein that confers a wide range of functions through its multiple domains: its protein-binding NHL and b-box domains allow it to act as an adapter for multiple translational repressor complexes (*e.g.*, Sxl, Nanos (Nos), Argonaute-1 (AGO1), see figs S1-2 and tables S1-2). Its E3-ubiquitin ligase domain likely enables it to modulate proteolysis [38]. Given *mei-P26's in vitro* role in

infection [37] and its *in vivo* role in GSC maintenance [38], differentiation [39,40], and meiosis [40,41], we selected it as a candidate gene for modulating *w*Mel-host interactions.

We report that *D. melanogaster* flies infected with the *w*Mel strain of *Wolbachia* partially rescue *mei-P26* mutations and exhibit reinforced fertility. In flies homozygous for hypomorphic *mei-P26*, infection with *w*Mel elevates fertility in both males and females to a level sufficient to maintain a stable stock, whereas the uninfected stock is unsustainable. Infection rescues GSC maintenance and cyst differentiation by mitigating the downstream effects of perturbed *mei-P26* function on other protein and mRNA expression. Specifically, *w*Mel infection restores a wild-type-like expression profile for phosphorylated Mothers against decapentaplegic (pMad), Sxl, Bam, and Oo18 RNA-binding (Orb) proteins, as well as *tut* and *bgcn* mRNAs. We find evidence of *w*Mel's beneficial reproductive manipulator abilities in OreR wild-type flies, illustrating how bacterially-mediated developmental resilience may be selected for in nature. These results are essential to understanding how *w*Mel reaches high frequencies in natural *D. melanogaster* populations and these beneficial functions may be able to be harnessed for biological control applications.

Results

Here, we explore the effects of *w*Mel *Wolbachia* infection on *D. melanogaster's* essential fertility gene *mei-P26* through dosage knockdown with an RNAi construct, disrupted function with a hypomorphic allele, *mei-P26[1]*, and full knockdown with a null allele, *mei-P26[mfs1]*. Using fly fecundity assays, immunocytochemistry, and dualRNAseq, we show that *w*Mel can compensate for the loss of *mei-P26* to significantly rescue host fertility.

Infection with wMel rescues female D. melanogaster fertility in mei-P26 deficient flies

Infection with *w*Mel *Wolbachia* significantly rescued fertility defects induced by the loss of *mei-P26* function relative to the Oregon R (OreR) wild-type strain, as measured by offspring produced per female *D. melanogaster* per day (Fig 1A-E, fig S3; p<=2.2e-16 to 2.9e-2, Wilcoxon rank sum test; see tables S2-6). Offspring production requires successful maintenance of the GSC, differentiation of a GSC daughter cell into a fully developed and fertilized egg, embryogenesis, and hatching into a first-instar larva. Breaking offspring production down into egg lay and egg hatch components (Fig 1B,C) revealed that as allelic strength increased, from *nos*-driven RNAi to hypomorphic and null alleles, fertility impacts shifted from those that impacted differentiation/development (egg hatch) to those that also impacted egg production (egg lay).

Infection with *w*Mel mediated a significant degree of fertility rescue for all allelic strengths and nos:GAL4>UAS-driven RNAi knockdowns, suggesting a robust bacterial rescue mechanism that compensates for loss of protein dosage and function. Rescue was more than complete for *nos*-driven *mei-P26* RNAi depletion (from 26% deficient offspring production in uninfected flies): *w*Mel-infected *mei-P26* RNAi females produced 44% more offspring than infected OreR wild-type females (37 versus 25 larvae/female/day, p<=1.15E-02 Wilcoxon rank sum test, table S4 and Fig 1A,E) due to a higher rate of egg production (p<=6.99E-05 Wilcoxon rank sum test, table S5 and Fig 1B,E), opposed to a higher hatch rate (Fig 1C,E and table S6). This may suggest a synergistic function between *w*Mel and low-dose *mei-P26* in the GSC. In uninfected and *w*Mel-infected *mei-P26[1]* hypomorphic females, offspring production decreased 94% and 73%, respectively, compared to OreR wild-type of the matching infection status (p<=2.26E-14 and 3.45E-12 Wilcoxon rank sum test, respectively, table S4 and Fig 1A,E). Comparing uninfected and *w*Mel-infected female *mei-P26[1]* fecundity revealed that *w*Mel infection increases the number of offspring produced per day (1.6 versus 7 larvae/female/day, p<=9.37E-05 Wilcoxon rank sum test, table S4 and Fig 1A) through increasing both the rate of egg lay (p<=2.82E-02 Wilcoxon rank sum test, table S5 and Fig 1B) and egg hatch (p<=2.55E-03 Wilcoxon rank sum test, table S6 and Fig 1C). In uninfected and *w*Mel-infected *mei-P26[1]/mei-P26[mfs1]* trans-heterozygous females, offspring production decreased 99% and 82%, respectively, relative to OreR wild-type (p<=3.40E-04 and 5.01E-10 Wilcoxon rank sum test, table S4 and Fig 1A,D). Comparing uninfected and *w*Mel-infected trans-heterozygous flies showed that infection elevates offspring production (0.2 versus 4.6 larvae/female/day, p<=1.03E-05 Fisher's exact test, table S4 and Fig 1A) through increasing the rate females lay eggs (p<=4.71E-05 Wilcoxon rank sum test; Fig 1B) and the rate those eggs hatch (p<=4.20E-03 Wilcoxon rank sum test; table S6 and Fig 1C). In females homozygous for the most severe allele, *mei-P26[mfs1]*, offspring production decreased 100% and 97% in uninfected and *w*Mel-infected flies relative to wild-type, respectively (p<=5.14E-06 Fisher's exact test, table S4 and Fig 1A). Offspring

production was marginally rescued in *mei-P25[mfs1]* flies by *w*Mel infection (0 (uninfected) versus 0.76 (infected) larvae/female/day, p<=5.14E-06 Fisher's exact test, table S4, Fig 1A), in part due to infected flies laying eggs at a higher rate than uninfected flies (p<=3.04E-05 Wilcoxon rank sum test, Fig 1B). However, no female laid 20 or more eggs in one day, precluding an estimation hatch rate rescue (Fig 1C). See Supplemental Methods, tables S2-6, and fig S3 for a full description of the fecundity assays and data.

*w*Mel-mediated *mei-P26* rescue is robust and sufficient to rescue this gene in a stable stock. Infection with *w*Mel elevates the number of offspring produced per day across the fly lifespan in *mei-P26[1]* hypomorphic and *nos*-driven RNAi-knockdown females (p<=1.5e-11 to 3.4e-2 Kolmogorov-Smirnov Test, table S7 and Fig 1F,G). However, the underlying number of eggs laid per day and the hatch rate do vary considerably with age for both infection states and genotypes (fig S4A-D). The *w*Mel rescue mechanism is not specific to females, as the weaker impacts of *mei-P26* loss on male fertility are mitigated by *w*Mel-infection (fig S4E-G; p<=6.1e-6 to 2.9e-2 Wilcoxon rank sum test, tables S3-S5). Thus, we were able to establish a homozygous stock of *mei-P26[1]* flies infected with *w*Mel *Wolbachia.* In contrast, the uninfected stock only lasted a few generations without balancer chromosomes (Fig S4H,I). Given the severe, yet significantly rescuable nature of the *mei-P26[1]* allele (Fig 1A-C and fig S2B,D), we proceeded with this genotype for many of our subsequent assays for specific immunocytological rescue phenotypes.

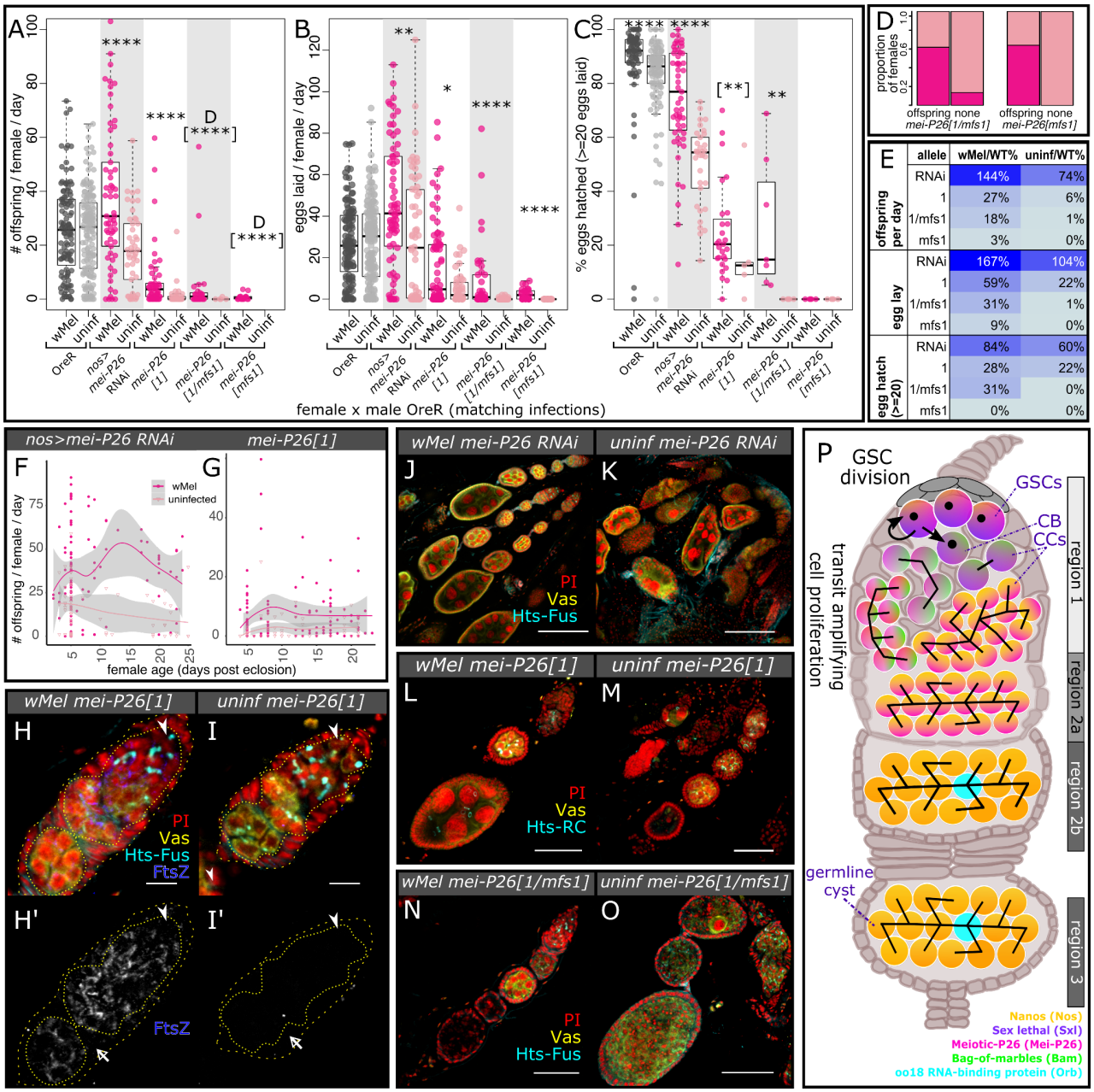

	allele	wMel/WT%	uninf/WT%
offspring per day	RNAi	144%	74%
	1	27%	6%
	1/mfs1	18%	1%
	mfs1	3%	0%
egg lay	RNAi	167%	104%
	1	59%	22%
	1/mfs1	31%	1%
	mfs1	9%	0%
egg hatch (>=20)	RNAi	84%	60%
	1	28%	22%
	1/mfs1	31%	0%
	mfs1	0%	0%

Fig 1. *w*Mel infection rescues the loss of essential host fertility gene *mei-P26* in females (and males, see Fig S4E-G). A-C) Beeswarm boxplots of A) overall offspring production, broken into B) eggs laid and C) eggs hatched, from single female RNAi, hypomorphic, and null *mei-P26* knockdown female flies crossed to single OreR males of the same infection state and age (3-7 days old). The null allele *mei-P26[mfs1]* reduced egg lay rates in both transheterozygotes and homozygotes below an average of 20 for both infected and uninfected females, necessitating an analysis of females with and without offspring (see D). Wilcoxon rank sum test *p<=0.05, **<=0.01, ***<=0.001, ****<=1e-4. Fisher's exact test [**]p<=0.01, [****]<=1e-4. D-E) D) Bar plots of the proportion of female samples of the indicated genotypes with offspring and without offspring, infected and uninfected with *Wolbachia*. E) Table listing the percentage of wild-type fecundity demonstrated by *w*Mel-infected (left) or uninfected (right) *mei-P26* mutants in order of increasing severity, from top to bottom (see also tables S4-6). Cell values from low to high proportions are colored from light to dark blue, respectively. F-G) Knockdown *mei-P26 D. melanogaster* fecundity versus female age, fit with a local polynomial regression (dark gray bounds=95% confidence intervals). Infection with *w*Mel increases offspring production over the first 25 days of the (F) *mei-P26* RNAi and (G) *mei-P26[1]* hypomorphic female lifespan. H-O) Confocal mean projections of *D. melanogaster* ovarioles and germaria. H-I') Intracellular *w*Mel FtsZ localizes to germline (yellow, Vas+, inner dotted outline) and somatic (Vas-, space between inner dotted and outer dashed outlines)

cells at high titers, with low background in uninfected flies. Bacteria are continuously located in the *mei-P26[1]* germline, starting in the germline stem cell (GSC) (arrowhead near Hts-bound spectrosome). Somatic cell regions are indicated with empty arrowheads. J-O) Cytology reveals that *w*Mel-infection rescues J,K) *mei-P26* RNAi, L,M) *mei-P26[1]* (see also fig S5), and N,O) *mei-P26[mfs1]*-induced oogenesis defects. Fluorescence channels were sampled serially and overlaid as indicated on each set of Figs as follows: cyan=anti-Hu Li Tai Shao (Hts), yellow=anti-Vasa (Vas), blue=*w*Mel anti-Filamenting temperature-sensitive mutant Z (FtsZ), and red=propidium iodide (PI) DNA staining. Scale bars: H-I'=10 μm, L-O=50 μm, J-K=100 μm. J) Diagram of a wild-type *D. melanogaster* germarium, highlighting key events and cell types by region as in [42]. Somatic cells in beige, GSC-derived cells are brightly colored gradients leading to differentiated cyst cells in yellow, with specified oocytes in blue. The black structure that originates in the GSC is the spectrosome, which becomes a branching fusome as the cystoblast (CB) is formed, moves away from the niche, and divides into cystocytes (CCs).

Female germline morphology is rescued by wMel infection in mei-P26 deficient flies

In the *D. melanogaster* germarium, *w*Mel is continuously present at high titers in both germline and somatic cells (Fig 1H-H', compared to control in Fig 1I-I'), consistent with previous reports [26,27,43]. The bacteria localize more strongly to the germline-derived cells than the somatic cells (co-localization of FtsZ and Vas in Fig1H-H'). Intracellular *w*Mel can be identified in the GSC, the cystoblast (CB), the cystocytes (CCs), and the developed cyst. This positioning puts *w*Mel in all of the critical cell types and stages that *mei-P26* is active, enabling the bacterium to compensate for *mei-P26's* developmental functions in GSC maintenance and differentiation.

Comparing the cytology of *mei-P26* knockdown oocytes infected and uninfected with *Wolbachia* confirmed that *w*Mel-infected ovarioles exhibit far fewer developmental defects than uninfected, more closely resembling OreR wild-type (Fig 1J-O and fig S5 versus Fig 1P; Vasa (Vas)=germline [44], Hu Li Tai Shao (Hts)=cytoskeletal spectrosome/fusome [45], propidium iodide (PI)=DNA). Specifically, *w*Mel infected *mei-P26*-knockdown ovarioles exhibited more normally-formed cysts, consisting of somatically-derived follicle cells surrounding germline-derived nurse cells and an oocyte, than uninfected ovarioles. Aberrant phenotypes included cysts lacking the follicle cell exterior (Fig 1K,M), the germline-derived interior (Fig 1M,N), or a normal number of differentiated nurse cells (Fig 1O).

These comparative data for a range of *mei-P26* alleles, RNAi-knockdowns, and host ages indicate that *w*Mel rescues *mei-P26's* developmental functions in early host oogenesis. In contrast, *w*Mel does not rescue *mei-P26*'s role in meiosis. Segregation defects were not rescued by *w*Mel infection, as indicated by elevated X-chromosome nondisjunction (NDJ) rates in both infected and uninfected *mei-P26[1]* homozygous hypomorphs (NDJ=7.7% and 5.6%, respectively, Fig S6A,B). In the following sections, we analyze *w*Mel's ability to rescue *mei-P26* function at each of the critical timepoints in early oogenesis.

Host GSCs are maintained at higher rates in wMel-infected than uninfected mei-P26-deficient flies

GSCs were quantified by immunofluorescence staining of the essential GSC markers phosphorylated Mothers Against Dpp (pMad) and Hu Li Tai Shao (Hts) in "young" 4-7 day old (Fig 2) and "aged" 10-13 day old females (fig S7A-C). Positive pMad staining indicates the cell is responding to quiescent signals from the surrounding somatic GSC niche cells. Positive Hts staining requires localization to a single punctate spectrosome, opposed to a branching fusome [46].

Staining revealed an increase in the average number of GSCs per *mei-P26[1]* germarium with *w*Mel infection, relative to uninfected germaria in young, 4-7 day old flies (infected/hypomorph: 1.0 vs uninfected/hypomorph: 0.58, $p<=2.9e-4$ Wilcoxon rank sum test, table S8), but GSC maintenance did not reach OreR wild-type rates (infected/WT: 2.3 and uninfected/WT: 1.9, $p<=1.2e-4$ to $2.8e-4$ Wilcoxon rank sum test, Fig 2A-E and table S8). *w*Mel-infected *mei-P26[1]* germaria also had more cells manifesting other GSC properties, such as a large cytoplasm and physical attachment to the cap cells of the somatic niche [46], than uninfected germaria. In contrast to the *mei-P26[1]* allele, RNAi knockdown of *mei-P26* did not significantly affect the numbers of GSCs per germarium (infected/RNAi: 2.1 and uninfected/RNAi: 1.9, S7A-C and table S8), suggesting that the modest

reductions in *mei-P26* dosage have a stronger impact on differentiation than GSC maintenance. OreR wild-type germaria did not exhibit different numbers of GSCs due to *w*Mel infection (Fig 2C-E and table S8).

The number of GSCs per germarium in *w*Mel-infected *mei-P26[1]* females converges on OreR wild-type values in aged 10-13 day old germaria (fig S7C). As wild-type flies age, the number of GSCs per germarium declines naturally [47], even in *w*Mel-infected flies (aged/infected/WT: 1.6 versus young/infected/WT: 2.3, p<=0.019 Wilcoxon rank sum test, Fig 2C-E, fig S7C, and table S8). Both infected and uninfected *mei-P26[1]* females appear to retain some of their GSCs as they age (aged/infected/hypomorph: 1.5 and aged/uninfected/hypomorph: 0.94, p<=0.013-0.014 Wilcoxon rank sum test, fig S7C and table S8). While OreR wild-type infected and uninfected flies lose from 3% to 31% of their GSCs in the first two weeks, infected and uninfected *mei-P26[1]* flies increase their GSC abundance by 43% and 63% in this time (fig S7C), potentially through recruiting differentiated GSCs [48]. Taking both age-dependent trajectories in GSC retention into account, by the time *w*Mel-infected *mei-P26[1*] germaria are 10-13 days old, they contain the same average number of GSCs per germarium as wild-type flies and significantly more GSCs than uninfected *mei-P26[1]* flies (p<=0.015 Wilcoxon rank sum test, fig S7C and table S8). Therefore, *Wolbachia* enhances stem cell maintenance in both young and old *mei-P26[1]* females.

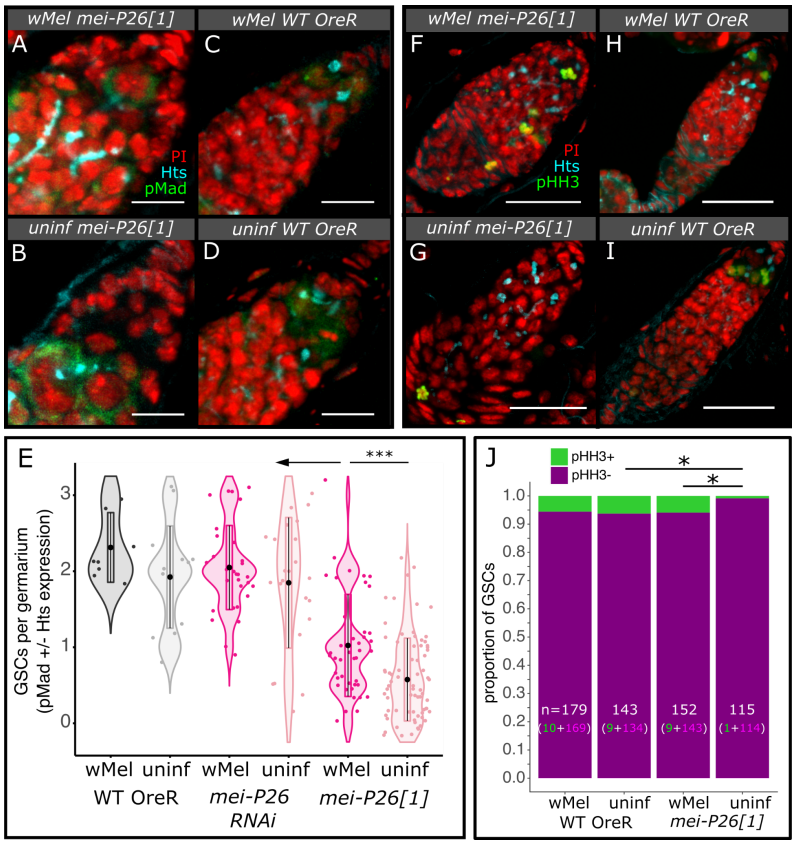

Fig 2. *w*Mel infection rescues *mei-P26*-induced defects in female GSC maintenance. A-E) Infection with *w*Mel confers higher numbers of GSCs per germarium in *mei-P26[1]* germaria than in uninfected flies. A-D) Confocal mean projections of *D. melanogaster* germaria stained with antibodies against Hts and pMad. E) Violin plots of the number of GSCs per germarium. As fully functional GSCs express pMad and have Hts-labeled spectrosomes, each was weighted by half and allows for partial scores. Wilcoxon rank sum test *=p<0.05, **=0.01, ***=0.001, ****=1e-4. F-J) Mitotic GSCs detected by phospho-histone H3 (pHH3) expression revealed that *w*Mel restored mitosis in hypomorphic *mei-P26* GSCs relative to uninfected GSCs. F-I) Confocal mean projections of *D. melanogaster* germaria stained with antibodies against Hts and pHH3. J) Stacked bar chart of the proportion of GSCs found expressing pHH3 in female germaria. Fisher's exact test *=p<0.05. Fluorescence channels were sampled serially and overlaid as indicated on each set of Figs as follows: cyan=anti-Hts, yellow=anti-Vas, red=PI, green=anti-pMad in A-D and anti-pHH3 in F-I. Scale bars A-D=10 μm and F-I=25 μm.

Infected *mei-P26[1]* GSCs are functional, as indicated by their ability to divide by mitosis (Fig 2F-J and table S9). We identified nuclei in mitosis by positive anti-phospho-histone H3 serine 10 (pHH3) staining, a specific marker of Cdk1 activation and mitotic entry [49]. Significantly fewer GSCs were in mitosis in uninfected *mei-P26[1]* germaria than infected *mei-P26[1]* and uninfected OreR wild-type germaria (0.09% versus 6%, p=4.7e-2 and 4.6e-2 Fisher's exact test, Fig 2F-J and table S9). There was no difference in the frequency of GSCs in mitosis between uninfected and infected wild-type germaria (5-6%, Fig 2H-J and table S9). Mitotic cystoblasts and cystocytes were only significantly enriched in infected *mei-P26[1]* germaria compared to infected wild-type germaria (p<=1.3e-2 Wilcoxon rank sum test, fig S7D and table S10), despite over-replication during transit-amplifying (TA) mitosis being a common phenotype in uninfected *mei-P26[1]* germaria (discussed below and [50]).

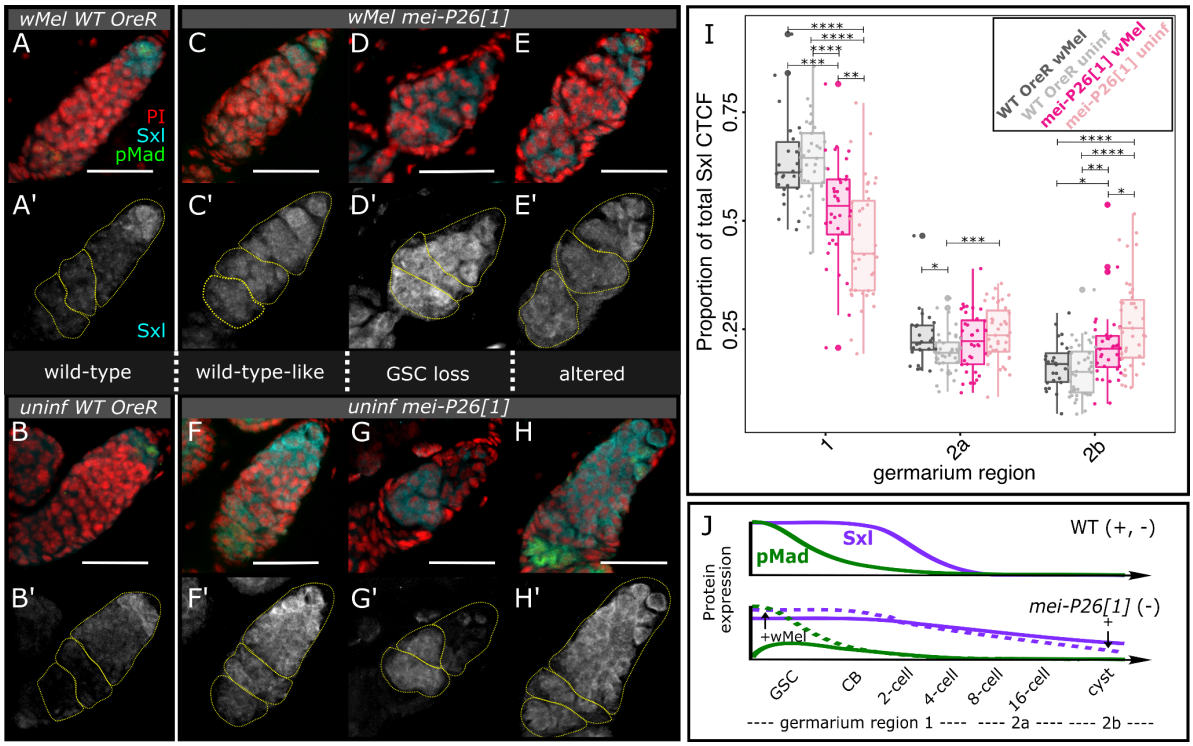

Fig 3. Infection with *w*Mel mitigates the consequences of dysfunctional *mei-P26* on *Sxl* expression in the germarium. A-H') Confocal mean projections of *D. melanogaster* germaria stained with antibodies against Sxl and pMad. Three phenotypes for each *mei-P26[1]* infection state are shown, (left) one as similar to wild-type as possible, (middle) one representative of GSC loss, pMad-negative, and (right) one representative of a developmentally altered phenotype retaining pMad-positive GSCs. We sampled the fluorescence channels serially and overlaid them as indicated on each set of Figs: cyan=anti-Sxl, red=PI, green=anti-pMad. Scale bars=25 μm. I) Bar-scatter plots of relative Sxl fluorescence expression levels across the germarium, by region. Colors as labeled in Figs 1A-D and 2E, from left to right: dark gray=*w*Mel-infected OreR, light gray=uninfected OreR, dark pink=*w*Mel-infected *mei-P26[1]*, light pink=uninfected *mei-P26[1]*. Wilcoxon rank sum test *=p<0.05, **=0.01, ***=0.001, ****=1e-4. J) Model of *w*Mel Sxl expression rescue in *mei-P26[1]* germaria. Green dashed line represents *w*Mel's upregulation of pMad expression in the GSC (Fig 2A-E). Purple dashed line represents *w*Mel's upregulation of Sxl in the GSC/CB and downregulation of Sxl by germarium region 2b. Arrows with + symbols indicate *w*Mel's action on gene expression.

<u>*Regulation of host Sxl expression is rescued in wMel-infected germaria*</u>

Proper Sxl expression is required for GSC maintenance and differentiation [51]. High levels of Sxl in the GSC maintains stem cell quiescence [52]. When the GSC divides and the cystoblast (CB) moves away from the niche, Sxl cooperates with Bam and Mei-P26 to bind to the *nos* 3' untranslated region (UTR) and downregulate Nos protein levels to promote differentiation [50,53].

We quantified Sxl localization patterns in whole ovaries stained with anti-Sxl antibodies by confocal microscopy of whole oocytes, revealing that Sxl dysregulation due to *mei-P26* loss is mitigated by *w*Mel infection (Fig 3). Less Sxl is expressed in uninfected *mei-P26[1]* germarium region 1 and more Sxl is expressed across regions 2a and 2b, relative to OreR wild-type (p<=5.7e-10 to 5.3e-5 Wilcoxon rank sum test, Fig 3A-B' vs F-H' and I, fig S7E, and table S11). Infection with *w*Mel increased Sxl expression in germarium region 1, had no impact on region 2a, and suppressed expression in region 2b relative to uninfected *mei-P26[1]*, replicating an expression pattern similar to that seen in wild-type germaria (p<=5.7e-10 to 8.4e-3 Wilcoxon rank sum test, Fig 3A-B' vs C-E' and I, fig S7E, and table S11). Interestingly, *w*Mel infection may impact Sxl expression in OreR germaria, as the protein is significantly elevated in region 2a of *w*Mel-infected relative to uninfected germaria (Fig 3I). Thus, Sxl dysregulation due to *mei-P26* loss can be partially-rescued by the presence of *w*Mel, suggesting that *w*Mel's mechanism for *mei-P26* rescue may underlie how Nos regulation in *w*Mel-infected Sxl mutants [31,34].

Bam expression is partially restored in wMel-infected mei-P26 mutant germaria

In wild-type female flies, Bam expression begins immediately after the cystoblast daughter cell moves away from its undifferentiated sister, which remains bound to the GSC niche ([50,54] and illustrated in Fig 1J). Bam binds to the fusome and stabilizes CyclinA to promote TA mitosis, producing 16 cyst cells from a single CB [55]. Immediately following these four mitoses, Bam expression is down-regulated in wild-type ovaries to limit germline cysts to sixteen germline-derived cells.

Through anti-Bam immunofluorescence confocal imaging and quantification, we determined that *w*Mel-infection mitigates aspects of Bam dysregulation in *mei-P26[1]* germaria (Fig 4). Loss of Mei-P26 deregulates and extends Bam expression past germarium region 1 (Fig 4A-B" versus C-F" and G, fig S7F, and table S12), producing excess nurse-like cells [50]. Infection with *w*Mel enables Bam upregulation at the CB-to-16-cell stage in *mei-P26[1]* germaria relative to uninfected germaria (p<=0.016, Fig 4G). Bam may also be downregulated in stage 2a and 2b *w*Mel-infected *mei-P26[1]* germaria because uninfected germaria express significantly more Bam than wild-type (p<= 0.019 Wilcoxon rank sum test, Fig 4G and table S12), whereas wMel-infected germaria do not (Fig 4G and table S12). Unfortunately, variance in *mei-P26[1]* Bam fluorescence intensity among samples is too large to resolve whether uninfected and infected germaria differ in Bam expression after the 16-cell stage with this dataset.

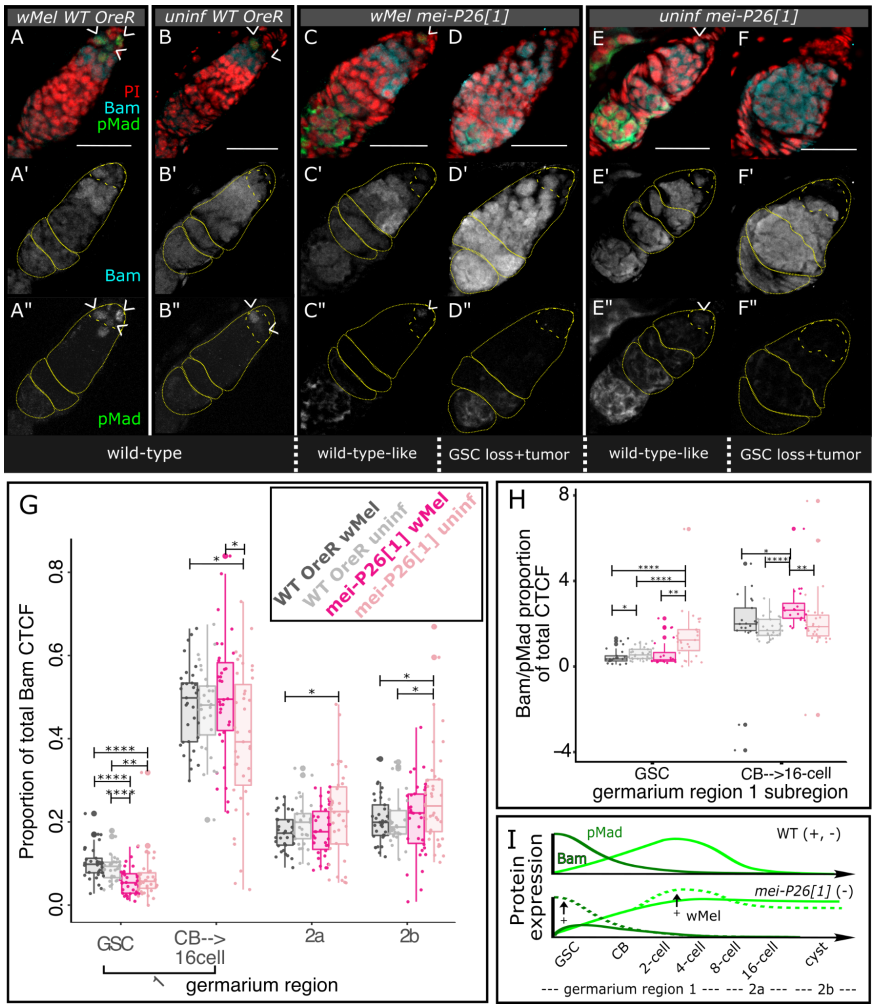

Fig 4. Infection with *w*Mel mitigates the consequences of dysfunctional *mei-P26* on *Bam* expression in the germarium. A-F") Confocal mean projections of *D. melanogaster* germaria stained with antibodies against Bam and pMad. Two phenotypes for each *mei-P26[1]* infection state are shown, (left) one as similar to wild-type as possible and (right) one representative of developmentally altered phenotypes. G) Bar-scatter plots of relative Bam fluorescence expression levels across the germarium, by region. We subdivided region 1 into GSC and CB/cystocyte subsections because Bam expression ramps up in the CB. H) Bar-scatter plot of the ratio of relative Bam to pMad fluorescence. As pMad and Bam expression is mutually exclusive in the GSC and CB/cystocytes, respectively, OreR wild-type values are near zero. Values significantly higher than this reflect dysregulation of the stem cell state. I) Model of *w*Mel rescue of Bam expression in *mei-P26[1]* germaria. Colors as labeled in Figs 1A-C, 2E, and 3I, from left to right: dark gray=*w*Mel-infected OreR, light gray=uninfected OreR, dark pink=*w*Mel-infected *mei-P26[1]*, light pink=uninfected *mei-P26[1].* Wilcoxon rank sum test *=p<0.05, **=0.01, ****=1e-4. Scale bars=25 μm.

Infection with *w*Mel alters Bam expression in the GSC and CB to achieve an expression profile similar to and more extreme than wild-type germaria, respectively (Fig 4H-I). Both infected and uninfected *mei-P26[1]* germaria exhibit lower Bam expression than wild-type in the GSC niche (Fig 4G). This contrasts with expectations from the literature: bone morphogenic protein (BMP) signaling from the somatic niche induces pMad expression in the GSC, which directly represses Bam transcription, preventing differentiation [56]. Loss of *mei-P26* function in the GSC should derepress Brat, resulting in pMad repression, and inappropriate Bam expression [38]. However, we see lower Bam expression in both *w*Mel-infected and uninfected *mei-P26[1]* GSCs relative to OreR wild-type (p<=1.3e-6 to 1.4e-3 Wilcoxon rank sum test, Fig 4G and table S13). The elevated relative Bam/pMad expression ratio in uninfected *mei-P26[1]* GSCs (p<=2.5e-4 to 4.0e-4 Wilcoxon rank sum test, Fig 4H-I and table S13) may explain this departure from expectations. Although GSC Bam expression is lower than in wild-type, Bam expression is clearly dysregulated and upregulated relative to pMad

expression, as expected for germline cells that have lost their stem cell identity [57,58]. Normalizing against pMad expression also reinforces the finding that *w*Mel elevates Bam expression even higher than wild-type levels in *mei-P26[1]* hypomorphs at the CB-to-16-cell stage (p<=1.2e-6 to 2.0e-2 Wilcoxon rank sum test Fig 4H-I and table S13).

<u>*w*Mel rescues normal germline cyst and oocyte development impaired by *mei-P26* knockdown</u>
Mei-P26-deficient flies over-proliferate nurse cells and partially-differentiate GSCs to produce tumorous germline cysts ([38,39] and Fig 5A-D vs E-H, Fig 5I, and table S14). In RNAi knockdown ovaries, the formation of tumorous germline cysts is significantly mitigated by *w*Mel infection (35.3% vs 16.3% of cysts with more than 15 nurse cells, respectively; p=4.5e-3 Fisher's exact test, Fig 5E-F vs G-H and table S14). In contrast, germline cyst tumors found in *mei-P26[1]* allele germaria were not rescued by *w*Mel infection, despite the bacterium's ability to rescue the rate at which these eggs hatch into progeny (Fig 5I vs Fig 1A,C), but consistent with their dysregulation of Bam expression in germarium regions 2a and 2b (Fig 4G). The stronger nature of the *mei-P26[1]* allele relative to the nos-driven RNAi knockdown likely underlies the difference in the number of tumorous cysts. Lack of tumor rescue indicates that either tumorous cysts produce normal eggs at some rate or *w*Mel infection rescues tumors later in oogenesis, perhaps through some somatic mechanism [59–62].

Overexpression of *mei-P26* produces tumors in both uninfected and infected ovaries, however, infected ovaries exhibit significantly more tumors than uninfected ovaries (p=1.6e-3 Fisher's exact test, Fig 5I and table S14). Finding that an excess of *mei-P26* recapitulates the tumorous phenotype induced by a lack of *mei-P26* indicates that this gene exerts a concentration-dependent dominant negative effect on its own function. Given that infection with *w*Mel makes this dominant negative phenotype more severe, we hypothesize that *w*Mel may make a factor that acts to enhance Mei-P26 function, potentially through a direct interaction or redundant function.

Infection with *w*Mel increases the rate of oocyte-specific Orb localization in *mei-P26[1]* germline cysts (Fig 5J-R, fig S7G, and table S15), suggesting that *w*Mel rescues functional cyst formation. Oocyte specification in region 2a of the germarium (see diagram in Fig 1J) is inhibited by the loss of *mei-P26* through the derepression of *orb* translation [38]. Mei-P26 binds to the *orb* 3' UTR and prevents its translation. Following cyst patterning and development, one of the 16 germline-derived cells is designated as the oocyte through specific oo18 RNA-binding protein (Orb) expression [63]. In region 2a, the germline cyst cell fated to become the oocyte activates *orb* translation [38]. Loss of *mei-P26* results in *orb* derepression and non-specific expression [38]. Infection with *w*Mel restores oocyte-specific Orb expression in *mei-P26[1]* cysts relative to uninfected cysts (p=5.9e-9 Fisher's exact test, Fig 5L-N' vs O-Q' and table S15). We observed oocyte-specific Orb staining 93-94% of the time in wild-type cysts, whereas *mei-P26[1]* reduced this frequency to 25%, and *w*Mel infection recovered *mei-P26[1]* cysts to 61% (counts in table S15). Oocyte-specific expression of Orb in *w*Mel-infected cysts is robust, even in those that are developmentally aberrant (*e.g.*, the double oocyte in Fig 5M-M'). These results suggest that *w*Mel rescues oocyte-specific Orb translation enhancing or duplicating Mei-P26's function in *orb* translational repression.

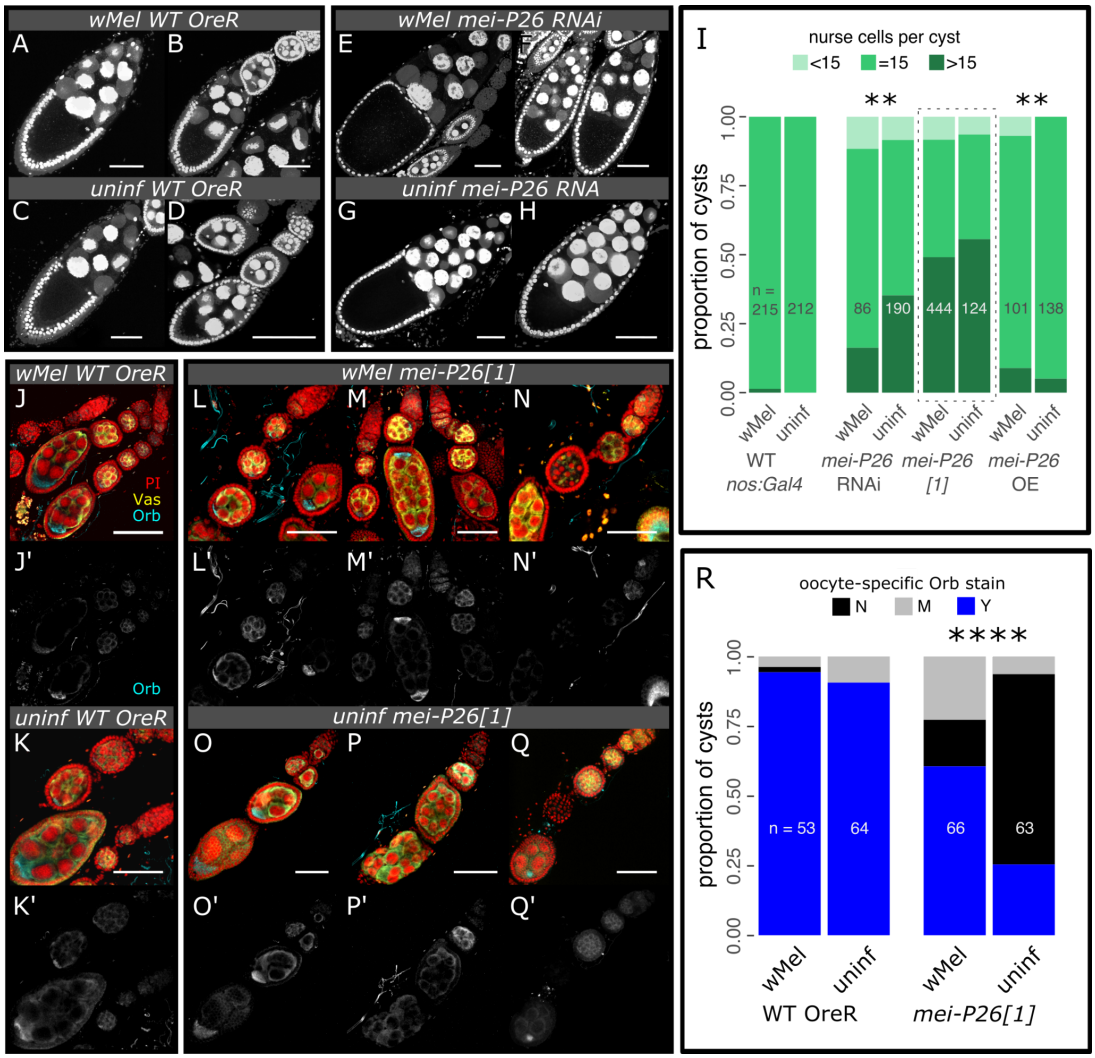

Fig 5. *w*Mel infection rescues cyst tumors and restores oocyte specification in *mei-P26* mutants. A-I) Loss and over-expression of Mei-P26 induces the formation of tumorous cysts, which contain more than 15 nurse cells. *w*Mel infection mitigates *nos*>RNAi-knockdown and exacerbates *nos*>overexpression (OE) phenotypes. A-H) Confocal max projections of ~25 µm-thick sections of *D. melanogaster* oocyte cysts stained with PI. I) Stacked bar chart of the proportion of germline cysts containing an abnormal number of nurse cells (less than or greater than 15 nurse cells). J-R) Hypomorphic *mei-P26[1]* cysts infected with *w*Mel significantly restored Orb translational regulation relative to uninfected cysts. Oocyte specification occurs in regions 2b-3 of the germarium (see diagram in Fig 1J), when Orb expression becomes restricted to the nascent oocyte. J-Q') Confocal mean projections of *D. melanogaster* germaria stained with antibodies against Orb and Vas. R) Stacked bar chart of the proportion of germline cysts containing oocyte-specific Orb staining. Sample sizes are written on the bar charts. N=no, M=maybe, and Y=yes. Fisher's exact test **=p<1e-2, ****=p<1e-4. Scale bars=50 µm.

OreR wild-type host fertility is beneficially impacted by wMel infection

Consistent with *w*Mel's ability to rescue the partial to complete loss of essential germline maintenance genes encompassing a range of functions, we discovered that this intracellular symbiont can reinforce fertility in *D. melanogaster* stocks displaying full wild-type fertility (Fig 1C, fig S8A-C, and table S4-6). We analyzed egg lay, egg hatch, and overall offspring production rates independently to detect *w*Mel effects on multiple components of fertility. Overall offspring production per female per day was elevated in *w*Mel-infected nos:Gal4/CyO females relative to uninfected females by 49% (27 (uninfected) vs 40 (infected) offspring/female/day, p<=2.2e-3 Wilcoxon rank sum test, fig S8A and table S4). Infection with *w*Mel increased the number of eggs laid per female per day for the nos:Gal4/CyO balancer stock by 49% (42 vs 28 eggs/female/day, p<=2.2e-3 Wilcoxon rank sum test, fig S8B and table S4), but did not have any detectable effect on egg lay rates in other genotypes

with wild-type fertility. Following embryogenesis, infection with *w*Mel elevated the rate that OreR and nos:Gal4/CyO wild-type eggs hatch into L1 stage larvae by 5.2% and 2.5%, respectively (88 and 91% (infected) versus 83 and 89% (uninfected) of eggs hatched, p<=1e-4 to 2.1e-3 Wilcoxon rank sum test, Fig 1C, fig S8C, and table S6). These results suggest that beneficial impacts of *w*Mel infection are evident, yet variable among *D. melanogaster* stocks with wild-type fertility.

We measured OreR fertility across its lifetime (~50 days), and found that *w*Mel may produce higher lifetime fecundity relative to uninfected flies (Fig 6A-C and table S7). OreR females were aged as indicated along the x-axis of Fig 6A-C and mated to 3-7 days old males of matching infection status. *w*Mel-infection maintains elevated OreR egg hatch rates as flies age (p<=7.1e-9 Kolmogorov-Smirnov test, Fig 6C and table S6), while maintaining similar levels of egg production as uninfected flies (Fig 6B and table S6). This culminates in age ranges in which infected flies may produce an excess of offspring relative to uninfected flies (see gap between the regression confidence intervals when flies were ~20-30 days old, Fig 6A). The efficiency gains imparted on hosts by infection-induced elevated hatch rates could potentially accumulate for higher lifetime fitnesses, as resources are more efficiently converted to offspring.

Immunostaining of anti-FtsZ confirms that *w*Mel exhibits high titers in the OreR wild-type germarium and concentrates in the oocyte in early cysts (Fig 6D-F'). The intracellular bacteria are continuously located in the germline, starting in the GSC and proceeding through the end of embryogenesis and fertilization. Thus, *w*Mel are located in the right place at the right time to reinforce female host fertility through interactions with the GSC and oocyte cyst, as well as to correct for perturbations caused by male CI-related alterations [64].

The *w*Mel strain of *Wolbachia* in its native *D. melanogaster* host exhibits weak CI that decreases with age (fig S9A-D), suggesting low maintenance of CI mechanisms [8]. Mating *w*Mel-infected OreR males to infected and uninfected OreR virgin females revealed that *w*Mel reduces uninfected egg hatch by 26% when males are zero to one day old (p<=4.6e-4 Wilcoxon rank sum test, fig S9A and table S6), but this moderate effect is eliminated by the time males are five days old, on average (fig S9C and table S6). Only young males significantly impact offspring production (p<=1.7E-2 Wilcoxon rank sum test, fig S9B,D and table S4). In contrast, the *Wolbachia* wRi strain that naturally infects *Drosophila simulans* and induces strong CI [10,65], reduces uninfected egg hatch by 95% when males are zero to one day old (p<=5.6e-8 Wilcoxon rank sum test, fig S9E and table S6) and only loses some of this efficacy by five days (75% hatch reduction, p<=3.6e-4, Wilcoxon rank sum test; fig S9G, table S6). This significantly impacts overall offspring production (p<=6.5E-7 and 5.0E-2 Wilcoxon rank sum test, fig S9F,H and table S4). Paternal grandmothers of CI offspring were 3-7 days old, contributing to weak CI in the *D. melanogaster* crosses [17]. Overall, these results suggest that *w*Mel's beneficial reproductive manipulations may affect its fitness more than its negative reproductive manipulations in nature.

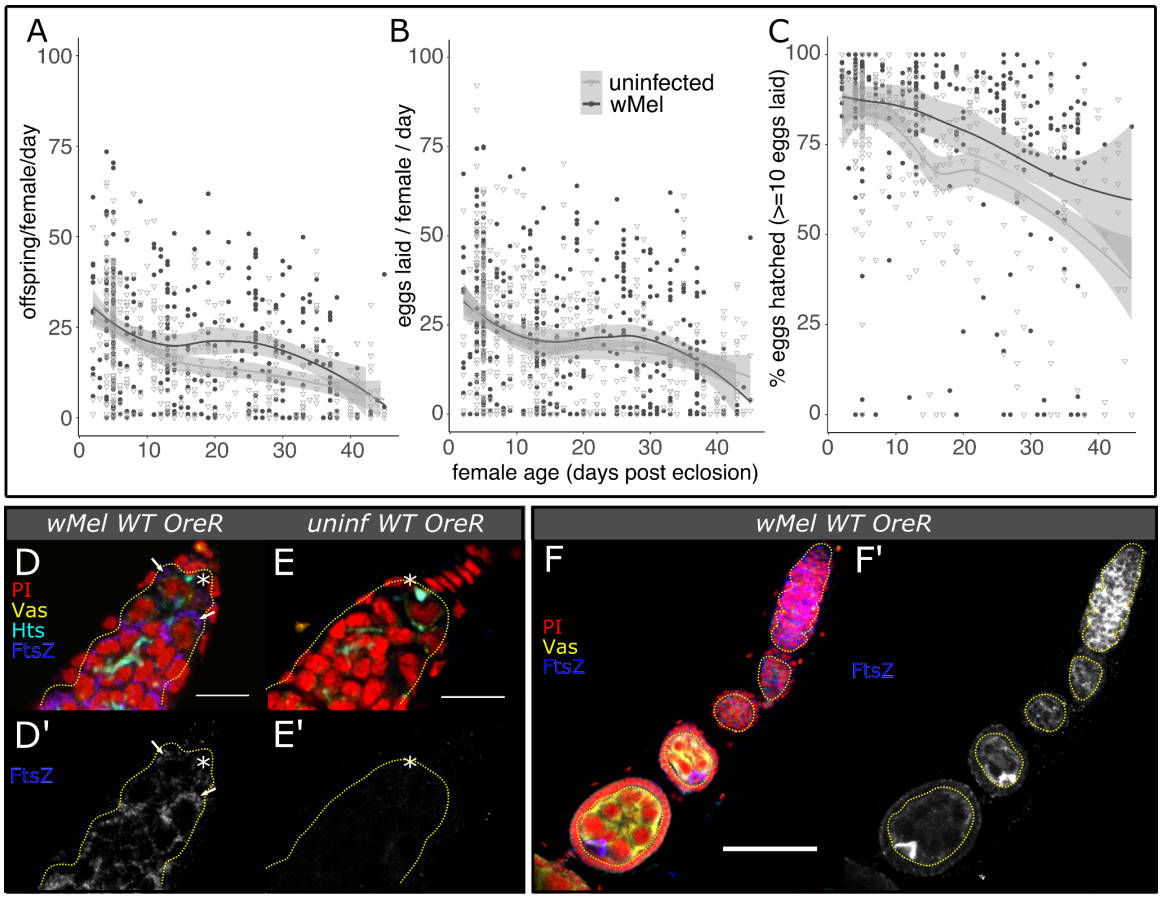

Fig 6. The *w*Mel strain of *Wolbachia* reinforces OreR wild-type fertility. A-C) *D. melanogaster* OreR fecundity versus female age, fit with a local polynomial regression (dark gray bounds=95% confidence intervals). Infection with *w*Mel may elevate A) offspring and B) egg offspring production at time points during the host lifespan through continuously elevating C) hatch rate. D-F') Confocal mean projections of *D. melanogaster* D-D') infected and E-E') uninfected germaria and F-F') an infected ovariole. Intracellular *w*Mel FtsZ localizes to germline (Vas+, outlined in dashed yellow) and somatic (Vas-) cells at high titers in infected OreR wild-type flies, with low background in uninfected flies. Bacteria in the GSC (* near the Hts-bound spectrosome) are indicated with arrows. Fluorescence channels were sampled serially and overlaid as indicated on each set of Figs as follows: cyan=anti-Hts, yellow=anti-Vas, blue=anti-FtsZ, and red=PI. Scale bars F-G=10 μm, H=50 μm.

<u>*w*Mel-mediated *mei-P26[1]* rescue may be enabled through rescuing and perturbing host transcription</u>
Exploring *w*Mel's effect on host gene expression in OreR and *mei-P26[1]* ovaries with dual-RNAseq (see Supplemental Methods and table S15) revealed that infection significantly alters host gene expression in a variety of ways (Fig 7A-C and table S16-19), which indicate a few potential mechanisms for *w*Mel-mediated fertility rescue. Of the 35344 transcripts in the *D. melanogaster* genome, 10720 were expressed at high enough levels in at least five of six samples one each genotype/infection group to be included in the analysis. Of the 1286 genes in the *w*Mel genome, 663 were expressed in *D. melanogaster* ovaries (Fig 7D and table S20).

Both uninfected and *w*Mel-infected hypomorphic *mei-P26[1]* ovaries exhibited a 5-fold depletion in *mei-P26* expression relative to OreR ovaries (fig S2B,D) and significant dysregulation in 1044 other genes due to the *mei-P26[1]* allele after FDR correction (Wald test FDR-adjusted p-value (padj)<= 0.05, Fig 7A,E, fig S10A, and table S17). The changes in gene expression due to the loss and dysfunction of *mei-P26* far outnumber and outpace the changes in gene expression due to infection, in either *D. melanogaster* genotype, and highlight how important *mei-P26* is as a global regulator of gene expression. This number is well in excess of the 366 genes thought to be involved in germline stem cell self-renewal [66], underscoring how many processes

mei-P26 is involved in, from germline differentiation [50] to somatic development [61]. Across biological process, cell component, and molecular function GO categories, loss of *mei-P26* impacted processes involving chromatin, recombination, protein-protein interactions, and muscle cell differentiation (fig S10B-G), supporting *mei-P26's* known role in genetic repression, differentiation, and meiosis [38,40,50].

Infection with *w*Mel significantly alters the expression of hundreds of *D. melanogaster* genes to either restore or compensate for *mei-P26*-regulated gene expression. We tested for genes significantly associated with infection state in DESeq2 under the full model: ~genotype + infection + infection*genotype, revealing 422 significantly differentially expressed genes (Wald test padj<=0.05, Fig 7B and table S18). Testing for an effect of the interaction between infection and genotype yielded another 20 significantly differentially expressed genes (Wald test padj<=0.05; Fig 7C, and tables S19). The most significantly differentially expressed genes are featured in Figure 7F-K and other significant genes are plotted in Fig 8 and figs S11-12. Binning gene expression patterns revealed that there are at least six main rescue gene expression phenotypes induced by *w*Mel-infection in mutant ovaries: full rescue, overshoot, undershoot, wild-type effect, inverse, and novel (Fig 7F-K, Fig8, fig S11A,B, and fig S12A,B). In "full rescue" phenotypes (Figs 7F and S11A), *mei-P26[1]* *w*Mel gene expression is indistinguishable from OreR levels and significantly different from uninfected *mei-P26[1]* levels. "Overshoot" phenotypes (Fig 7G) exhibit expression that is significantly in the opposite direction of the uninfected *mei-P26[1]* knockdown effect relative to OreR expression. Oppositely, "undershoot" phenotypes are partial corrections towards OreR expression in *mei-P26[1]* *w*Mel ovaries (Fig 7H). The one "wild-type effect" gene, an ER and Golgi cytoskeletal membrane anchor protein, demonstrated differential expression only between *w*Mel-infected and uninfected OreR ovaries (Fig 7I). Five genes exhibit "inverse" differential expression phenotypes, such as a sodium symporter (Fig 7J) and the transcription factor Chronophage (fig S12A), in which *mei-P26[1]* and OreR ovaries show opposite changes in differential expression relative to the uninfected genotype. In total, only these six "wild-type effect" and "inverse" genes were differentially expressed due to infection in OreR ovaries. Lastly, "novel" genes (Figure 7K) are those that only exhibit differential expression in *w*Mel-infected *mei-P26[1]* ovaries, suggesting a novel rescue or compensation pathway. For example, *suppression of retinal degeneration disease 1 upon overexpression 2* (*sordd2*) ubiquitin ligase mRNA expression is upregulated, without rescue, in both infected and uninfected *mei-P26[1]* ovaries (Fig 7E). One of the novel rescue candidates, SKP1-related C (*skpC*), is a down-regulated component of SCF ubiquitin ligase (Fig 7K), which might compensate for the upregulation of *sordd2.*

GO terms associated with infection and the interaction between infection and genotype (fig S11C-G, fig S12C-G, and Fig 8D) were consistent with *w*Mel's known ability to associate with host actin [67], microtubules, motor proteins [68–70], membrane-associated proteins [71], and chromatin [72]. Infection-associated genes were enriched in GO terms suggesting a cytoskeletal developmental function with chromatin interactions (fig S11C-G). Across biological processes, cellular compartment, and molecular function categories, genes were enriched in terms suggesting interactions with actin, myosin, contractile fibers, and muscle cell differentiation. Chromatin interactions were indicated by associations with condensin complexes, centromeres, and mitotic chromosomes. Genotype-by-infection interaction-associated genes were also enriched in cytoskeletal and chromatin-interaction GO terms, in addition to plasma membrane/cell junction-associated terms such as cell junction and synapse structure maintenance, cell cortex, and lipid and calmodulin binding (fig S12C-G). Interestingly, two chorion proteins (Fig 7F), an ecdysteroid 22-kinase associated protein (fig S11A), and an estrogen-related receptor (ERR) (fig S12A), which are likely involved in chorion formation [73], were rescued by *w*Mel. Considering that we have found *mei-P26[1]* embryos to have weaker corions then OreR wild-type embryos when treated with bleach, this finding suggests a novel chorion-associated function for *mei-P26* and a novel rescue phenotype for *w*Mel.

None of the 663 transcribed *w*Mel genes were significantly differentially expressed between the OreR and *mei-P26[1]* host genotypes, after p-values were FDR-corrected (Figure 7D, fig S13-14, and table S20), suggesting host regulation by *w*Mel's constitutively expressed genes. On average, *w*Mel transcriptomes were sequenced at 7.8-42.4x depth of coverage and *D. melanogaster* transcriptomes were sequenced at 25.9-35.9x (table S16). While these coverage ranges overlap, the 663 *w*Mel genes detected only spanned -1.5-fold depletion to 1.3-fold upregulation (table S20). In contrast, the 10720 expressed *D. melanogaster* genes spanned an order of magnitude more differential expression, with -10.041-fold depletion to 9.866-fold

upregulation (tables S17-S19). Thus, *w*Mel genes are weakly differentially transcribed compared to *D. melanogaster* genes, suggesting that *w*Mel may alter host phenotypes through downstream impacts of constitutively expressed proteins. To explore the constitutive effects of *w*Mel expression, we tested for GO pathway enrichment in the expressed transcriptome (fig S13). Pathways for DNA replication, protein expression, membrane transport, and heterotrophy (*e.g.*, oxidative phosphorylation) were detected in abundance. While many of these genes are likely involved in normal bacterial cell maintenance and replication, a significant enrichment in pathways for oxidative phosphorylation, translation, transcription, and membrane functions (fig S13A) suggest that some of these genes could be co-opted for host manipulation or processing host resources.

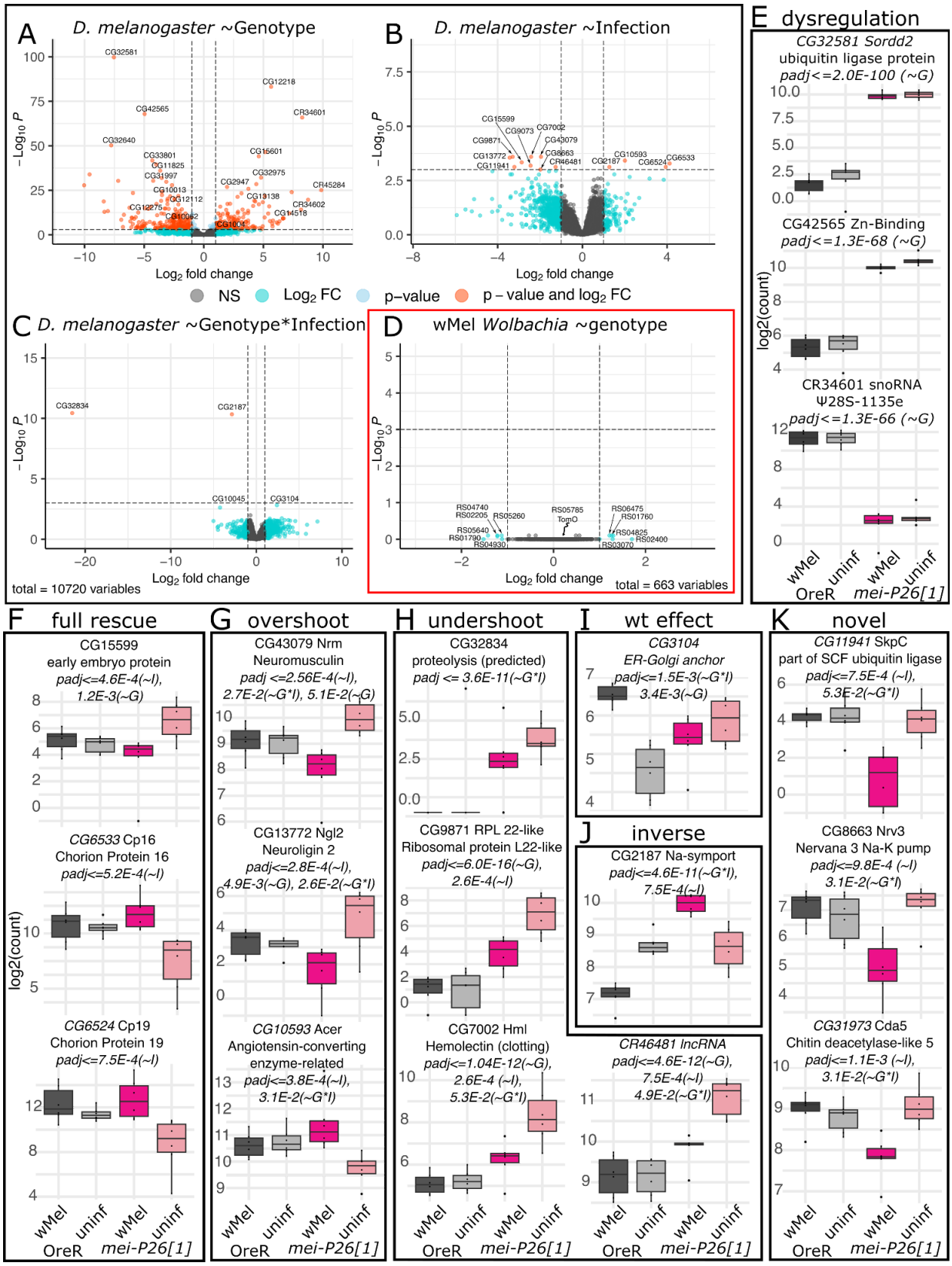

Fig 7. Differential expression analysis of *w*Mel and *D. melanogaster* genes from host ovaries reveal that *mei-P26* knockdown and infection influence global expression patterns. A-D) Volcano plots of log2-fold change in gene expression versus log10-FDR adjusted p-value (padj) for the test performed in each panel. E-K) Normalized transcript count plots for E) the three top genotype-associated (~*G*) Wald Test hits by padj, and F-K) *D. melanogaster* genes significantly associated (padj<=1e-3) with infection (~*I*) or jointly, genotype and

infection (~*G*I*), organized by the differential expression pattern. See Supplemental Figures S10-S13 for other significant and insignificant count plots. In all barplots, dark gray=*w*Mel-infected OreR, light gray=uninfected OreR, dark pink=*w*Mel-infected *mei-P26[1]*, light pink=uninfected *mei-P26[1].*

Among the 1044 significantly differentially regulated *D. melanogaster* genes impacted by *mei-P26* knockdown and infection were six genes (of 24) predicted in the literature (padj<=0.05 Wald test, and nine of 24 by p-value<=0.05; Fig 8, fig S1, and table S1-2). Loss of *mei-P26* function caused dysregulation in *oo18 RNA-binding protein* (*orb*), *gawky* (*gw*), *sex-lethal (sxl)*, *benign gonial cell neoplasm (bgcn)*, *tumorous testis (tut)*, and *bantam (mir-ban)* (padj<=0.05 Wald test, Fig 8C and * in Fig 8A,B). *Bam*, *Pumilio (pum)*, and *Justice Seizure (jus)* expression may be altered by *mei-P26* knockdown, but additional samples are needed to resolve high infection variance (*e.g.*, *mir-ban*) and low differential expression change (*e.g.*, *gw*) (p-value<=0.05 Wald test, Fig 8C and "*" in Fig 8A,B). Two of six genes exhibited evidence of *w*Mel rescue with an "undershoot" rescue phenotype ("r" in Fig 8 A,B)): *bgcn* and *tut* by padjust (Fig 8C). If we consider genes with significant unadjusted p-values, *gw* may also exhibit evidence of "undershoot" rescue (Fig 8C, "r" in Fig 8A). Bantam or *mir-ban* expression suppression may be rescued as well, but high variance among *w*Mel *mei-P26[1]* ovaries precludes DE rescue detection with this dataset (Fig 8C). In contrast, *orb, sxl*, *bam,* and *nos* transcript levels are not altered by *mei-P26* knockdown or *w*Mel infection, and therefore must be regulated post-transcriptionally. In total, these differential expression results reinforce and expand our understanding of how *w*Mel rescues and reinforces host reproduction at transcriptional and post-transcriptional levels.

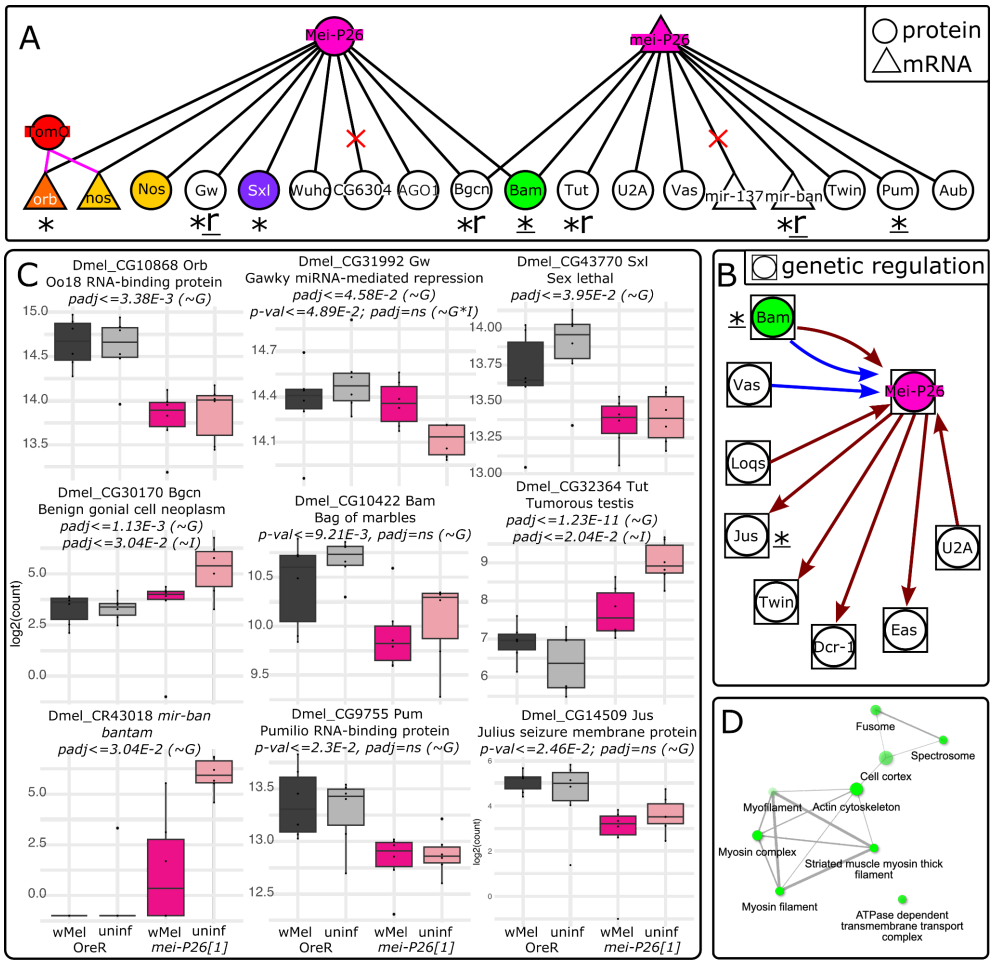

Fig 8. Mei-P26 interactions predicted from the literature are supported by our ovary dual-RNAseq results. A,B) Predicted *mei-P26* A) protein and mRNA physical interactions and B) genetic interactions. Symbols near gene names indicate significant DE interactions: *=significance by genotype; r=significance by infection, indicating a rescue phenotype; _=significance by uncorrected p-values only. Red "X"s in A indicate genes that were not expressed in our dataset (CG6304 and mir-137). C) Normalized transcript count plots for the genes designated

with symbols in A and B. In all barplots, dark gray=*w*Mel-infected OreR, light gray=uninfected OreR, dark pink=*w*Mel-infected *mei-P26[1]*, light pink=uninfected *mei-P26[1].* D) Cellular component GO terms for the 87 *(~G*I)* DE genes reveal an enrichment for early germline cytoskeletal structures and membrane proteins. Wald test association for listed padj and p-values are given in parentheses, as in Fig 7: genotype (~*G*), infection (~*I*), genotype*infection (~*G*I*).

Discussion

The *w*Mel strain of *Wolbachia* is a successful and widespread symbiont: naturally in *D. melanogaster* populations and novelly through lab-generated trans-infections of *w*Mel into non-native hosts used for biological control. However, we know remarkably little about the processes that shape how symbiont and host co-evolve and find mutually beneficial mechanisms for their reproduction. In this work, we confirm that *w*Mel's CI strength is typically weak in *D. melanogaster,* (fig 9A-D, [14–18]) and show that *w*Mel confers benefits on host fertility through reinforcing host germline stem cell maintenance and gamete differentiation (Figs 1-8).

Here, we demonstrate that *w*Mel infection can reinforce host fertility in both OreR wild-type and *mei-P26* mutants by correcting perturbed gene expression patterns, and we shed light on the long-standing mystery of how *w*Mel beneficially impacts host reproduction. Previously, *w*Mel was shown to rescue the partial loss of Sxl [31] and Bam [32], two essential genes for two very different stages of early oogenesis: GSC maintenance and CB differentiation and TA-mitosis, respectively. These findings left unresolved how *w*Mel suppresses these mechanistically and temporally distinct cellular processes, and suggested that *mei-P26* was not involved [31]. We show with an array of alleles and developmental assays that infection with *w*Mel rescues defects associated with mutant *mei-P26,* a gene required for both GSC maintenance and differentiation. Infection with *w*Mel rescues all stages of oogenesis in *mei-P26* RNAi knockdowns, as well as hypomorphic and null alleles (Fig 1-5 and 7-8, figs S4-8 and S11-12, and tables S4-S15 and S18-S19). Mei-P26 is a TRIM-NHL protein that regulates gene expression via mRNA translational inhibition through the Nos mRNA-binding complex, interactions with the RNA-induced silencing complex (RISC), and protein ubiquitination [38,74]. Importantly, Mei-P26 interacts with Sxl in the GSC and CB and Bam in the CB and cystocytes [36,50]. These interactions suggest that the mechanism *w*Mel employs to rescue *mei-P26* function may also be responsible for rescuing aspects of Sxl-dependent GSC maintenance and CB differentiation and Bam-dependent cyst differentiation.

In this in-depth molecular and cellular analysis of *w*Mel-mediated manipulation of GSC maintenance and differentiation, we discovered that *w*Mel rescues *mei-P26* germline defects through correcting perturbed pMad, Sxl, Bam, and Orb protein expression and *bgcn* and *tut* mRNA expression towards OreR wild-type levels (diagrammed in Fig 9A). Infection with *w*Mel partially rescued GSC-specific pMad expression relative to wild-type flies (Fig 2A-E), suggesting that the bacteria restored BMP signaling from the somatic germline stem cell niche [38]. Finding that these cells are also able to divide (Fig 2F-J), further supports their functionality and stemness. Given that *mei-P26* is likely involved in *Drosophila* Myc (dMyc) regulation, and overexpression of dMyc induces competitive GSCs [75], *w*Mel's GSC rescue mechanism may involve dMyc upregulation. Although, our transcriptomic data indicate that dMyc is not rescued at the transcriptional level (fig S15 and tables S17-19). In the germline cells that left the niche, *w*Mel recapitulated the properly timed changes in pMad, Sxl, and Bam expression that are normally influenced by *mei-P26* and are required during cystoblast differentiation to form the 16-cell germline cyst [39,40,50,74] (Fig 3-4, S5E,F). While Bam downregulation is not fully rescued by wMel (Fig 4), finding that *tut* mRNA expression is partially reduced in wMel-infected *mei-P26[1]* germaria (Fig 8) suggests that there may be an unreported regulatory interaction between Tut, Bam, and Mei-P26 in females [76], which could rescue the overexpression of Bam in late germline cyst development.

This is the first time *w*Mel has been found to rescue oocyte differentiation post-cyst formation, suggesting that *w*Mel has pervasive impacts throughout oogenesis that may reinforce embryogenesis. We confirmed the downstream consequences of Bam expression rescue in *w*Mel-infected *mei-P26[1]* ovaries by finding fewer germline cyst tumors in infected flies (Fig 5A-I). These germline cysts appeared to be functional, based on restored oocyte-specific expression of the essential oocyte differentiation protein Orb in infected *mei-P26[1]* cysts, relative to uninfected cysts (Fig 5J-R). Finding that *w*Mel rescues Cp16 and Cp19 chorion protein, *tut,*

bgcn, and other transcript expression in ovary tissues (Figs 7F-8 and figs S11-12) further supports the conclusion that *w*Mel can rescue the downstream impacts of *mei-P26* loss. Future work is needed to explore how the overshoot and novel DE categories mitigate the loss of *mei-P26*, which may occur through some alternate or compensatory pathway. In addition to the mechanism discussed previously for ubiquitin ligase rescue, the loss of Ionotropic receptor 76a (Ir76a) or nicotinic Acetylcholine Receptor α5 (nAChRα5) expression (fig S10A) could be rescued by the novel upregulation of the Wunen-2 lipid phosphate phosphatase as a receptor or membrane transporter in wMel-infected *mei-P26[1]* ovaries (fig S12B). These functions could underlie *w*Mel-induced developmental resilience in OreR embryogenesis, as demonstrated by elevated hatch rates in *w*Mel-infected OreR flies (Fig 1C and 6C).

The *w*Mel strain's rescue of *D. melanogaster mei-P26* is likely independent of the *Wolbachia* TomO protein. Prior work on TomO indicates that the bacterial protein's primary mode of action is through destabilizing ribonucleoprotein (RNP) complexes [35] (diagrammed in Fig 9B). This is how TomO elevates Nos expression in the GSC [34] and how TomO inhibits the translational repressor Cup from repressing Orb translation in mid-oogenesis (stage 8) [35,77]. In contrast, Mei-P26 interacts with Ago1 RISC to inhibit Orb translation through binding the *orb '3-UTR miRNA* binding sites [38]. Although Mei-P26 and TomO produce opposite outcomes for Orb expression and TomO is not significantly upregulated in *mei-P26[1]* ovaries (fig S14C), TomO-*orb* binding may underlie *w*Mel's ability to rescue Orb repression, if *w*Mel produces other factors that modulate the interaction. Alternatively, *w*Mel may make another RNA-binding protein. Given that Sxl is also repressed through the *sxl* 3'-UTR by Bruno [78], such a protein could be involved in restoring Sxl regulation in *mei-P26* mutants. Neither *orb* or *sxl* expression is rescued at the mRNA level by *w*Mel infection (Fig 8C), lending further support for rescue at the translational or protein-interaction/modification level.

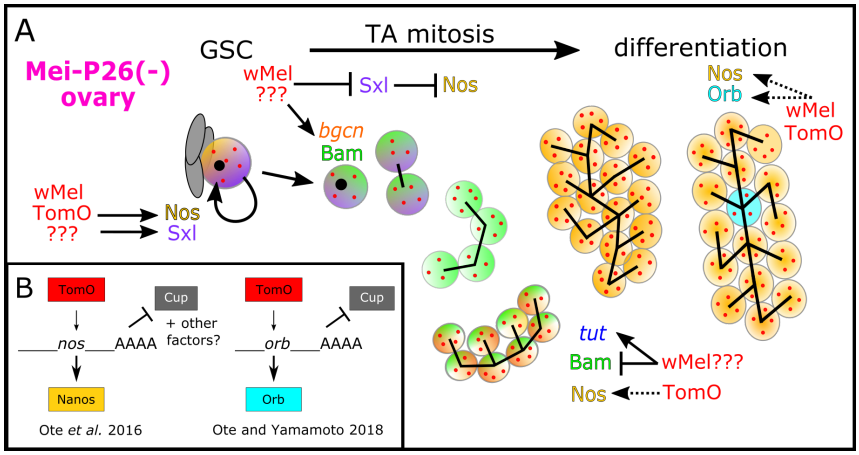

Fig 9. Model of *w*Mel's interactions with essential host genes in early GSC maintenance and germline cyst formation. A) In *mei-P26* mutants, *w*Mel restores normal Bam, Sxl, and Orb expression through various mechanisms, most of which are unknown (???=unknown *w*Mel factors). Protein and mRNA expression rescue correlates with cytological rescue from GSC maintenance through germline cyst differentiation. B) Sxl rescue in the GSC is mediated through TomO's interaction with RNPs containing *nos* mRNA, upregulating Nos translation. Later, in stage 8 of cyst oogenesis, TomO was found to bind *orb* mRNA, displacing the translational repressor Cup, and upregulating Orb translation [34,35]. Dashed arrow in A indicates TomO's predicted function in enabling Orb derepression in early cyst differentiation. The factor that restores *mei-P26* repression of Orb translation in *mei-P26* mutants has not been identified.

Additional bacterial factors besides TomO must be involved in reinforcing host fecundity in wild-type flies and fertility mutants. First, Mei-P26 encodes three functional domains that confer at least three different functional mechanisms for modulating gene expression (mRNA-binding, miRNA-mediated, and ubiquitination). In a bacterial genome, these domains/functions are likely to be encoded by more than one protein [79]. Second, TomO rescues Sxl's GSC maintenance functions by binding *nos* mRNA, increasing levels of Nos translation, but it cannot fully rescue Sxl loss [34]. Immediately after the GSC divides to produce the CB, Sxl interacts with Bam, Mei-P26, Bgcn, and Wh to inhibit Nos translation [36,74]. Thus, a *w*Mel factor that inhibits Nos

translation, counteracting TomO's function to destabilize Nos translational repressors through RNA-binding [34,35], remains to be identified. Furthermore, Nos upregulation cannot explain Bam rescue because Nos and Bam exhibit reciprocal expression patterns during TA mitosis [36]. Third, exacerbation of the tumor phenotype induced by *nos:*Gal4-driven Mei-P26 overexpression by *w*Mel infection (Fig 5I) suggests that *w*Mel synthesizes a protein that directly mimics Mei-P26's functions in differentiation, and can reach antimorphic levels. Misregulated expression of a *mei-P26*-like factor could explain why *w*Mel-infected *mei-P26* RNAi females produce more eggs and offspring than OreR wild-type flies (Fig 1A,B). While TomO may recapitulate some of Mei-P26's functions, such as *orb*-binding, at least one other factor is needed to recapitulate proper Orb, Nos, and Bam regulation.

Understanding how *Wolbachia* interacts with host development at the molecular level is essential to deploying these bacteria in novel hosts and relying on vertical transmission to maintain them in host populations. CI has been a powerful tool for controlling host populations [80] and driving *Wolbachia* to high infection frequencies [3]. The continuous presence of bacterial reproductive manipulators in host germline stem cells opens the opportunity for compensatory developmental functions to evolve, as we have shown for *mei-P26.* While it is not known if any of the naturally occurring *mei-P26* alleles [32,81] confer loss of function that is remedied by the presence of *Wolbachia*, natural variation in developmental genes theoretically could have provided the selection pressure for *w*Mel to evolve its beneficial reproductive functions. Given that selection will favor the loss of CI if conflicting beneficial impacts on host fertility are realized [8], it is imperative that we understand the mechanisms underlying beneficial reproductive manipulations such as fertility reinforcement.

Materials and methods

Russell et al. *Wolbachia* endosymbionts manipulate GSC self-renewal and differentiation to enhance host fertility

Candidate gene selection

Leveraging what is known about wMel's abilities to rescue essential maintenance and differentiation genes [31,32] with empirical data on protein-protein and protein-mRNA interactions among these genes (esyN[82] networks in fig S1A-D and Fig 8; references in table S1) and data on interactions between host genes and wMel titers [37], we identified the essential germline translational regulator *meiotic P26* (*mei-P26*) as a potential target of of bacterial influence over germline stem cell (GSC) maintenance and differentiation pathways (fig S1A,B). Loss of *mei-P26* in uninfected flies produces mild to severe fertility defects through inhibiting GSC maintenance, meiosis, and the switch from germline cyst proliferation and differentiation [38–40].

***Drosophila* stocks and genetic crosses**

Flies were maintained on white food prepared according to the Bloomington Drosophila Stock Center (BDSC) Cornmeal Food recipe (aka. "white food", see https://bdsc.indiana.edu/information/recipes/bloomfood.html). The wMel strain of *Wolbachia* was previously crossed into two *D. melanogaster* fly stocks, one carrying the markers and chromosomal balancers w[1]; Sp/Cyo; Sb/TM6B, Hu and the other carrying the germline double driver: P{GAL4-Nos.NGT}40; P{GAL4::VP16-Nos.UTR}MVD1. These infected double balanced and ovary driver stocks were used to cross wMel into the marked and balanced FM7cB;;;sv[spa-pol], null/hypomorphic mutants, and UAS RNAi TRiP lines to ensure that all wMel tested were of an identical genetic background. The *D. melanogaster* strains obtained from the Bloomington Drosophila Stock Center at the University of Indiana were: Oregon-R-C (#5), w1118; P{UASp-mei-P26.N}2.1 (#25771), y[1] w[*] P{w[+mC]=lacW}mei-P26-1 mei-P26[1]/C(1)DX, y[1] f[1]/Dp(1;Y)y[+]; sv[spa-pol] (#25716), y[1] w[1] mei-P26[mfs1]; Dp(1;4)A17/sv[spa-pol] (#25919) , y[1] sc[*] v[1] sev[21]; P{y[+t7.7] v[+t1.8]=TRiP.GL01124}attP40 (#36855). We obtained the UASp-mRFP/CyO (1-7M) line from Manabu Ote at the Jikei University School of Medicine. *Drosophila simulans w[-]* stocks infected with the Riv84 strain of wRi and cured with tetracycline were sourced from Sullivan Lab stocks[83,84]. All fly stocks and crosses were maintained at room temperature or 25C on white food (BDSC Cornmeal Food) because the sugar/protein composition of host food affects *Wolbachia* titer[84].

Wild-type fertility stocks: Paired wMel-infected (OreR_wMelDB) and uninfected Oregon R (OreR_uninf) stocks were made by crossing males of Oregon-R-C to virgin females from paired infected and uninfected balancer

stocks of the genotype w[1];CyO/Sp;Hu/Sb. To ensure that no differences arose between these two *D. melanogaster* genotypes during the balancer cross or subsequently, we backcrossed males of the OreR_wMelDB stock to females of the OreR_uninf stock for ten generations and repeated egg lay and hatch assays (F10_OreR_uninf). Paired infected and uninfected nosGal4/CyO and nosGal4/Sb flies were made by crossing to paired infected and uninfected balancer stocks, as described above.

The genomic and phenotypic consequences of the *mei-P26* alleles studied here and previously (e.g., [31]) have been characterized [40]. The hypomorphic *mei-P26[1]* allele was created by the insertion of a P{lacW} transposon in the first intron of *mei-P26*, which codes for the RING domain. The mostly null *mei-P26[fs1]* allele tested by Starr and Cline in 2002 was generated by a second P{lacW} insertion in *mei-P26[1]'s* first insertion. The fully (male and female) null *mei-P26[mfs1]* allele arose by deleting the P{lacW} insertion from *mei-P26[1]*, along with ~2.5 kb of flanking sequence. According to Page et al. 2000, these three alleles form a series, with increasing severity: *mei-P26[1]* < *mei-P26[fs1]* (and other fs alleles) < *mei-P26[mfs1]*.

Fecundity crosses

Overview: SLR performed the 3002 fecundity crosses continuously between October 2020 and January 2022, in batches based on their eclosion date (raw data in table S2). Infected and uninfected OreR lines were maintained continuously to 1) control the age of grandmothers of CI males, 2) regularly have OreR virgins for *mei-P26* and CI fecundity assays, 3) collect and age WT females for the aged fertility assay, and 4) obtain large sample sizes from *mei-P26* fertility mutants. The full fecundity dataset is contained in table S2 and plotted in fig S3.

Fecundity cross category	**Female age**	**Male age**	**Parallel control crosses**
wMel-infected mei-P26 rescue	3-7 days old	3-7 days	Uninfected and wild-type
wMel-infected OreR wild-type	3-7 days old	3-7 days	Uninfected OreR wild-type and other "wild-type" fertility stocks (e.g., nos:Gal4/CyO)
aged wMel-infected mei-P26 rescue	2-25 days old	3-7 days	Uninfected and wild-type
aged wMel-infected OreR wild-type	2-45 days old	3-7 days	Uninfected OreR wild-type
cytoplasmic incompatibility in wMel-*D.melanogaster* OreR	3-7 days old	0 or 3-7 days (from 3-7 day old mothers)	Rescue, reciprocal, and uninfected
cytoplasmic incompatibility in wRi-*D.simulans w[-]*	3-7 days old	0 or 3-7 days (from 3-7 day old mothers)	Rescue

Cross conditions: Food (vials of Bloomington's white food recipe), laying media (grape food), and incubation conditions were made in-house in large batches monthly. Grape spoons: Approximately 1.5 mL of grape agar media (1.2x Welch's Grape Juice Concentrate with 3% w/v agar and 0.05% w/v tegosept/methylparaben, first dissolved at 5% w/v in ethanol) was dispensed into small spoons, allowed to harden, and stored at 4°C until use. Immediately prior to use in a cross, we added ground yeast to the surface of each spoon.

Preparation of flies for fecundity crosses: Paired wMel-infected and uninfected genetic crosses were performed in parallel for the four *mei-P26* mutants (RNAi, [mfs1], [1], [mfs1/1]) to produce homozygous virgin females of both infection states for parallel fecundity crosses. Mutant genetic crosses were performed multiple (three or more) times across the 14 months to produce homozygotes from many different parents and matings. CI crosses were performed with males from infected grandmothers that were 3-7 days old. Males were aged either 0 (collected that day) or 5 days, depending on the cross. We collected males from vials over multiple days, so the majority of males were not the first-emerged.

Virgin female flies collected for fecundity crosses were transferred to fresh food and aged an average of 5 days at room temperature (from 3 to 7), or longer for the aged OreR, *mei-P26 RNAi*, and *mei-P26[1]* fecundity crosses. Males and virgin female flies were stored separately and males were aged zero or 3-7 days. Long-term aged virgin females were kept as small groups in vials of fresh white food. Every few days the vials were inspected for mold and flies were moved on to fresh food.

Fecundity cross protocol: In the afternoon of the first day of each cross, one male and one female fly were knocked out on a CO_2 pad, added to a vial containing a grape spoon, allowed to recover, and then transferred to a 25°C constant humidity incubator on a 12 light/dark cycle to allow for courting and mating. The following day, each spoon was replaced with a fresh spoon, and the vials were returned to 25°C for more mating. On the third day, we removed the flies from the vials, counted the number of eggs laid on the spoon's grape media, and replaced the spoon in the vial at 25°C for two days. After approximately 40 hours, we counted the number of hatched and unhatched eggs. The exact times and dates for all steps in all crosses were recorded (table S2) and plotted to show consistent results across the timeframe (fig S3).

Fecundity cross analysis: Fecundity data were parsed using perl scripts and plotted in R. Individual crosses were treated as discrete samples. Hatch rates were calculated from samples that laid 20 or more eggs (for 3-7 day old female plots) and 10 or more eggs (for age vs. hatch rate plots). Egg lay and offspring production rates were calculated from raw counts, divided by the fraction of days spent laying (metadata in table S2). Crosses with zero laid eggs (and offspring) were not rejected, as the fertility mutants often laid zero to few eggs. Our cross conditions were highly consistent and run daily, lending confidence to these zero-lay/offspring samples (figure S3). Drosophila fecundity vs female age data were fit in R using the stat_smooth loess method, formula y~x, with 0.95 level confidence interval.

Non-disjunction assays

We placed females homozygous for the *mei-P26[1]* allele bearing the yellow mutation (y[1] w[*] mei-P26[1] ;;; sv[spa-pol]) in vials with males bearing a wild-type yellow allele fused to the Y chromosome (y[1] w[1] / Dp(1;Y)y+). We made seven or eight vials of 1-10 females mated to a count-matched 1-10 males for infected and uninfected *mei-P26* hypomorphs, respectively. After eclosion, we screened for non-disjunction in the progeny by the presence of yellow males (XO) and normally colored females (XXY). Rates of non-disjunction (NDJ) were calculated to account for the inviable progeny (XXX and YO) with the equation NDJ rate = 2 *NDJ offspring / all offspring = (2XXY + 2X0)/(XX+XY+2XXY+2X0), as in [41].

Ovary fixation and immunocytochemistry

Within a day or two or eclosion, flies were transferred to fresh food and aged 3-7 days, or longer as indicated in the text. For long aging experiments, flies were transferred to fresh food every week and investigated for mold every few days. We dissected the ovaries from ~10 flies from each cross in 1xPBS and separated the ovarioles with pins. Ovaries were fixed in 600 µl heptane mixed with 200 µl devitellinizing solution (50% v/v paraformaldehyde and 0.5% v/v NP40 in 1x PBS), mixed with strong agitation, and rotated at room temperature for 20 min. Oocytes were then washed 5x in PBS-T (1% Triton X-100 in 1x PBS), and treated with RNAse A (10 mg/ml) overnight at room temperature.

After washing six times in PBS-T, we blocked the oocytes in 1% bovine serum albumin in PBS-T for one hour at room temperature, and then incubated the oocytes in the primary antibodies diluted in PBS-T overnight at 4C (antibodies and dilutions listed below). The following day, we washed the oocytes six times in PBS-T and incubated them in secondary antibodies diluted 1:500 in PBS-T overnight at 4C. On the final day, we washed the oocytes a final six times in PBS-T and incubated them over two nights in PI mounting media (20 µg/ml propidium iodide (PI, Invitrogen #P1304MP) in 70% glycerol and 1x PBS) at 4C. Overlying PI medium was replaced with clear medium, and oocytes were mounted on glass slides. Slides were stored immediately at -20C and imaged within a month. Infected and uninfected, as well as experimental and control samples were processed in parallel to minimize batch effects. Paired wMel-infected and uninfected OreR stocks were used as wild-type controls.

Primary monoclonal antibodies from the Developmental Studies Hybridoma Bank (University of Iowa) were used at the following dilutions in PBS-T: anti-Hts 1:20 (1B1)[45], anti-Vas 1:50[44], anti-Orb 1:20 (4H8)[63], anti-Bam 1:5[36], and anti-Sxl 1:10 (M18)[85]. Primary monoclonal antibodies from Cell Signaling Technology were used at the following dilutions: anti-Phospho-Smad1/5 (Ser463/465) (41D10) 1:300 (#9516S) and anti-Phospho-Histone H3 (Ser10) Antibody 1:200 (#9701S). Anti-*Wolbachia* FtsZ primary polyclonal antibodies were used at a 1:500 dilution (provided by Irene Newton). Secondary antibodies were obtained from Invitrogen: Alexa Fluor 405 Goat anti-Mouse (#A31553), Alexa Fluor 488 Goat anti-Rabbit (#A12379), and Alexa Fluor 647 Goat anti-Rat (#A21247).

Confocal imaging

Oocytes were imaged on a Leica SP5 confocal microscope with a 63x objective. Optical sections were taken at the Nyquist value for the objective, every 0.38 µm, at variable magnifications, depending on the sample. Most germaria were imaged at 4x magnification and ovarioles and cysts were imaged at a 1.5x magnification. Approximately 10 µm (27 slices) were sampled from each germarium and 25 µm (65 slices) were sampled from each cyst for presentation and analysis.

Propidium iodide was excited with the 514 and 543 nm lasers, and emission from 550 to 680 nm was collected. Alexa 405 was imaged with the 405 nm laser, and emission from 415 to 450 nm was collected. Alexa 488 was imaged with the 488 laser, and emission from 500 to 526 nm was collected. Alexa 647 was imaged with the 633 laser, and emission from 675 to 750 nm was collected.

Image analysis

Germaria and ovarioles were 3D reconstructed from mean projections of approximately 10 µm-thick nyquist-sampled confocal images (0.38 µm apart) in Fiji/ImageJ. Germline cyst developmental staging followed the standard conventions established by Spradling [86] and the criteria described below. We also scored and processed the confocal z-stacks for analysis as follows in the sections below.

GSC quantification: GSCs were scored by the presence of pMad and an Hts-labeled spectrosome in cells with high cytoplasmic volumes adjacent to the somatic germ cell niche and terminal filament [56]. When antibody compatibility prevented both pMad and Hts staining (*e.g.*, with anti-pHH3 staining), only one was used for GSC identification. The spectrosome was distinguished from the fusome by its position anterior of the putative GSC nucleus and the presence of a posterior fusome that continues into a posteriorly dividing cystoblast. We calculated the number of GSCs per germarium as the average number of pMad and Hts-spectrosome-expressing cells. Non-whole increments of GSCs indicate situations where a putative GSC expresses one attribute, but not the other.

Mitotic GSC quantification: Putative GSCs were identified as described above and scored for the presence of anti-phospho-Histone H3 (pHH3) staining. The number of pHH3-positive cystocytes in region 1 was also quantified across germaria.

Oocyte cyst tumor quantification: Using a 10x objective, we manually counted the number of nurse cells in each stage 6-10b cyst. Each count was repeated three times consistently and the cyst tallied as having less than 15, 15, or more than 15 nurse cells per cyst.

Bam and Sxl expression measured by fluorescence: We summed 27-slice nyquist-sampled z-stacks of each germarium in Fiji/ImageJ. Fluorescence intensity was measured by setting ImageJ to measure: AREA, INTEGRATED DENSITY and MEAN GRAY VALUE. Germarium regions were delimited as in [42] using Vas expression to indicate the germline. Three representative background selections were measured for subtraction. The corrected total cell fluorescence (CTCF) was calculated for each region of the oocyte as follows: CTCF = Integrated Density – Area of selected cell * Mean fluorescence of background readings. We controlled for staining intensity within a germarium and compared relative values among germaria.

Orb expression: Anti-Orb-stained oocyte cysts were manually scored for stage and Orb oocyte-staining in confocal z-stacks ImageJ.

Transcriptomics

We collected OreR and hypomorphic *mei-P26[1]* flies uninfected and infected with wMel and wMel-infected *nos:Gal4>UAS:mei-P26 RNAi* and nos:Gal4/CyO flies for RNAseq. Flies were collected after eclosion and moved to fresh food until they were 3-5 days old. Ovary dissections were performed in 1xPBS, in groups of 20-30 flies to obtain at least 10 mg of ovary tissue for each sample. After careful removal of all non-ovary somatic tissue, ovaries were promptly moved to RNAlater at room temperature, and then transferred to -80°C within 30 min for storage. Frozen tissue was shipped on dry ice to Genewiz Azenta Life Sciences for RNA extraction, cDNA synthesis, Illumina library preparation, and Illumina sequencing. The RNAi and control samples - both *nos:Gal4>UAS:mei-P26 RNAi* and *nos:Gal4/CyO* genotypes - were processed to cDNA with T-tailed primers, recovering only host transcripts. The *mei-P26[1]* and OreR samples were processed to cDNA using random hexamers and ribosomal sequences were depleted with sequential eukaryotic and bacterial rRNA depletion kits (Qiagen FastSelect). Illumina dual-indexed libraries were made from these cDNAs and sequenced as 2x150bp reads.

We processed and analyzed RNAseq datasets for differential expression using standard computational approaches and custom perl parsing scripts. Briefly, following demultiplexing, we trimmed adapter fragments from the RNAseq reads with Trimmomatic[87]. To generate sitewise coverage data to examine read alignments directly, we used the STAR aligner[88] and samtools[89], and plotted read depths across samples in R. We quantified transcripts by pseudoalignment with Kallisto[90]. The choice of reference transcriptome was key to recovering the maximum number of alignments: we merged the NCBI RefSeq assemblies for the wMel reference genome CDSs and RNAs from genomic (accession GCF_000008025.1) and the *D. melanogaster* reference genome RNAs from genomic (accession GCF_000001215.4; Release_6_plus_ISO1_MT) to obtain alignments against the full, non-redundant host-symbiont transcriptome. Simultaneous mapping to both genomes was performed to avoid cross-species mismapping[91]. This reference transcriptome was indexed at a kmer length of 31 in Kallisto (version 0.45.1)[90] and reads were pseudoaligned against this reference with the “kallisto quant” command and default parameters. Host and symbionts have distinct transcriptome distributions[92], necessitating the separation of the two transcriptomes prior to transcript normalization and quantification in DESeq2[93], which we performed with a custom perl script.

We imported the subset *D. melanogaster* and *w*Mel Kallisto transcriptome quantifications separately into R with Tximport [94] for DESeq2 analysis[93]. Transcript-level abundances were mapped to gene IDs to estimate gene-level normalized counts. For each transcriptome, we filtered out low-count/coverage genes across samples by requiring at least five samples to have a read count of 10 or more. We modeled interactions among our experimental groups as a function of genotype, infection, and the interaction between genotype and infection (~genotype + infection + genotype*infection) and performed Wald Tests to detect differential expression. Briefly, the maximum likelihood gene model coefficient for each gene’s expression count was calculated and divided by its standard error to generate a z-statistic for each gene under the full and reduced models. These z-statistics were compared to the values obtained under standard normal distribution for p-value calculations. FDR/Benjamini-Hochberg corrections were performed on these p-values to reduce the number of false positives. Normalized counts for each gene were output with the plotCounts() function in DESeq2 for plotting in R.

We manually investigated the top hits for each test for evidence of germline expression in the Fly Cell Atlas project[95] through Flybase. GO categories for differentially expressed genes returned from each DESeq2 Wald Test and tested for significance against the reference transcriptome set of IDs with ShinyGO0.77[96].

Transcriptomic data generated in this study are available through NCBI BioProjectnumber PRJNA992140.

Plotting and statistical analysis

Fecundity data were plotted, analyzed, and statistics were calculated in R. Differences in lay, hatch, and offspring production rates were evaluated with the nonparametric Wilcoxon Rank Sum test. When this was infeasible because non-zero samples were so few (*e.g.*, null alleles), we compared the binomially distributed categorical groups of females who laid or did-not-lay eggs with the Fisher's Exact test. All sample sizes, means, and p-values are presented in Table S2. Fecundity was plotted across fly ages and fitted with local polynomial regression. Single age pots were made with base R and the beeswarm[97] package and fecundity-vs-time plots were made with the ggplot2[98] package.

Confocal micrograph fluorescence intensities were analyzed, plotted, and statistics were calculated in R. Relative fluorescence intensities between oocyte genotypes were compared with the nonparametric Wilcoxon Rank Sum test. Counts of GSCs, mitotic GSCs, tumorous germline cysts, and orb-specific cysts were compared with Fisher Exact tests. Plots were made with the ggplot2[98] package.

We analyzed and plotted the dual-RNAseq results from Kallisto and DESeq2 in R. Bar and scatter plots were made with the ggplot2 package[98] and volcano plots were made with the EnhancedVolcano package (release 3.17)[99].

Acknowledgements: We thank the UCSC Life Sciences Microscopy Center (RRID:SCR_021135) and Ben Abrams for training and the use of their microscopes. We thank Irene Newton for aliquots of anti-*Wolbachia* FtsZ antibodies and Manabu Ote for a stock of UASp-mRFP/CyO (1-7M) flies. We thank Russ Corbett-Detig for his comments and feedback throughout this project. This work was supported by UC Santa Cruz, the UC Chancellor's Postdoctoral Fellowship, and the NIH (R00GM135583 to SLR; R35GM139595 to WTS).

Author Contributions:
SLR, study conception and design, data production and analysis, and writing. JRC, data production and analysis, and writing. WTS, study design and writing.

Supplementary Materials:
Supplementary Figures 1-15
Supplementary Tables 1-20

References:
1. Leftwich PT, Edgington MP, Chapman T. Transmission efficiency drives host–microbe associations. Proc R Soc B Biol Sci. 2020;287: 20200820. doi:10.1098/rspb.2020.0820
2. Bright M, Bulgheresi S. A complex journey: transmission of microbial symbionts. Nat Rev Microbiol. 2010;8: 218–230. doi:10.1038/nrmicro2262
3. Utarini A, Indriani C, Ahmad RA, Tantowijoyo W, Arguni E, Ansari MR, et al. Efficacy of Wolbachia-Infected Mosquito Deployments for the Control of Dengue. N Engl J Med. 2021;384: 2177–2186. doi:10.1056/NEJMoa2030243
4. Drown DM, Zee PC, Brandvain Y, Wade MJ. Evolution of transmission mode in obligate symbionts. Evol Ecol Res. 2013;15: 43.
5. Doremus MR, Hunter MS. The saboteur's tools: Common mechanistic themes across manipulative symbioses. Advances in Insect Physiology. Elsevier; 2020. pp. 317–353. doi:10.1016/bs.aiip.2020.03.003
6. Werren JH, Baldo L, Clark ME. *Wolbachia*: master manipulators of invertebrate biology. Nat Rev Microbiol. 2008;6: 741–751. doi:10.1038/nrmicro1969
7. Jansen VAA, Turelli M, Godfray HCJ. Stochastic spread of Wolbachia. Proc R Soc B Biol Sci. 2008;275: 2769–2776. doi:10.1098/rspb.2008.0914
8. Turelli M. Evolution of Incompatibility-Inducing Microbes and Their Hosts. Evolution. 1994;48: 1500. doi:10.2307/2410244
9. Weeks AR, Turelli M, Harcombe WR, Reynolds KT, Hoffmann AA. From Parasite to Mutualist: Rapid

Evolution of Wolbachia in Natural Populations of Drosophila. Keller L, editor. PLoS Biol. 2007;5: e114. doi:10.1371/journal.pbio.0050114
10. Carrington LB, Lipkowitz JR, Hoffmann AA, Turelli M. A Re-Examination of Wolbachia-Induced Cytoplasmic Incompatibility in California Drosophila simulans. Cordaux R, editor. PLoS ONE. 2011;6: e22565. doi:10.1371/journal.pone.0022565
11. Zug R, Hammerstein P. Bad guys turned nice? A critical assessment of *Wolbachia* mutualisms in arthropod hosts: *Wolbachia* mutualisms in arthropods. Biol Rev. 2015;90: 89–111. doi:10.1111/brv.12098
12. Kriesner P, Hoffmann AA, Lee SF, Turelli M, Weeks AR. Rapid sequential spread of two *Wolbachia* variants in *Drosophila simulans*. Charlat S, editor. PLoS Pathog. 2013;9: e1003607. doi:10.1371/journal.ppat.1003607
13. Ross PA, Axford JK, Yang Q, Staunton KM, Ritchie SA, Richardson KM, et al. Heatwaves cause fluctuations in wMel Wolbachia densities and frequencies in Aedes aegypti. Kohl A, editor. PLoS Negl Trop Dis. 2020;14: e0007958. doi:10.1371/journal.pntd.0007958
14. Hoffmann AA. Partial cytoplasmic incompatibility between two Australian populations of Drosophila melanogaster. Entomol Exp Appl. 1988;48: 61–67. doi:10.1111/j.1570-7458.1988.tb02299.x
15. Hoffmann AA, Hercus M, Dagher H. Population Dynamics of the Wolbachia Infection Causing Cytoplasmic Incompatibility in Drosophila melanogaster. Genetics. 1998; 11.
16. Reynolds KT, Hoffmann AA. Male age, host effects and the weak expression or non-expression of cytoplasmic incompatibility in Drosophila strains infected by maternally transmitted Wolbachia. Genet Res. 2002;80. doi:10.1017/S0016672302005827
17. Layton EM, On J, Perlmutter JI, Bordenstein SR, Shropshire JD. Paternal Grandmother Age Affects the Strength of *Wolbachia* -Induced Cytoplasmic Incompatibility in *Drosophila melanogaster*. Dubilier N, editor. mBio. 2019;10: e01879-19, /mbio/10/6/mBio.01879-19.atom. doi:10.1128/mBio.01879-19
18. Solignac M, Vautrin D, Rousset F. Widespread occurrence of the proteobacteria Wolbachia and partial cytoplasmic incompatibility in Drosophila melanogaster. Comptes Rendus Acad Sci - Ser III. 1994;317: 461–470.
19. Verspoor RL, Haddrill PR. Genetic Diversity, Population Structure and Wolbachia Infection Status in a Worldwide Sample of Drosophila melanogaster and D. simulans Populations. Welch JJ, editor. PLoS ONE. 2011;6: e26318. doi:10.1371/journal.pone.0026318
20. Kriesner P, Conner WR, Weeks AR, Turelli M, Hoffmann AA. Persistence of a *Wolbachia* infection frequency cline in *Drosophila melanogaster* and the possible role of reproductive dormancy: PERSISTENT *WOLBACHIA* FREQUENCY CLINE. Evolution. 2016;70: 979–997. doi:10.1111/evo.12923
21. Fry AJ, Palmer MR, Rand DM. Variable fitness effects of Wolbachia infection in Drosophila melanogaster. Heredity. 2004;93: 379–389. doi:10.1038/sj.hdy.6800514
22. Harcombe W, Hoffmann AA. Wolbachia effects in Drosophila melanogaster: in search of fitness benefits. J Invertebr Pathol. 2004;87: 45–50. doi:10.1016/j.jip.2004.07.003
23. Serga SV, Maistrenko OM, Matiytsiv NP, Vaiserman AM, Kozeretska IA. Effects of Wolbachia infection on fitness-related traits in Drosophila melanogaster. Symbiosis. 2021;83: 163–172. doi:10.1007/s13199-020-00743-3
24. Strunov A, Lerch S, Blanckenhorn WU, Miller WJ, Kapun M. Complex effects of environment and *Wolbachia* infections on the life history of *Drosophila melanogaster* hosts. J Evol Biol. 2022;35: 788–802. doi:10.1111/jeb.14016
25. Serga S, Maistrenko O, Rozhok A, Mousseau T, Kozeretska I. Fecundity as one of possible factors contributing to the dominance of the wMel genotype of Wolbachia in natural populations of Drosophila melanogaster. Symbiosis. 2014;63: 11–17. doi:10.1007/s13199-014-0283-1
26. Frydman HM, Li JM, Robson DN, Wieschaus E. Somatic stem cell niche tropism in Wolbachia. Nature. 2006;441: 509–512. doi:10.1038/nature04756
27. Toomey ME, Panaram K, Fast EM, Beatty C, Frydman HM. Evolutionarily conserved *Wolbachia*-encoded factors control pattern of stem-cell niche tropism in Drosophila ovaries and favor infection. Proc Natl Acad Sci. 2013;110: 10788–10793. doi:10.1073/pnas.1301524110
28. Foray V, Perez-Jimenez MM, Fattouh N, Landmann F. Wolbachia control stem cell behavior and stimulate germline proliferation in filarial nematodes. Dev Cell. 2018;45: 198–211. doi:10.1101/244046
29. Pannebakker BA, Loppin B, Elemans CP, Humblot L, Vavre F. Parasitic inhibition of cell death facilitates symbiosis. Proc Natl Acad Sci. 2007;104: 213–215.

30. Russell SL, Castillo JR. Trends in Symbiont-Induced Host Cellular Differentiation. In: Kloc M, editor. Symbiosis: Cellular, Molecular, Medical and Evolutionary Aspects. Cham: Springer International Publishing; 2020. pp. 137–176. doi:10.1007/978-3-030-51849-3_5
31. Starr DJ, Cline TW. A host–parasite interaction rescues Drosophila oogenesis defects. Nature. 2002;418: 76.
32. Flores HA, Bubnell JE, Aquadro CF, Barbash DA. The *Drosophila* bag of marbles gene interacts genetically with *Wolbachia* and shows female-specific effects of divergence. PLoS Genet. 2015;11: e1005453.
33. Bubnell JE, Fernandez-Begne P, Ulbing CKS, Aquadro CF. Diverse wMel variants of Wolbachia pipientis differentially rescue fertility and cytological defects of the bag of marbles partial loss of function mutation in Drosophila melanogaster. G3 GenesGenomesGenetics. 2021 [cited 2 Oct 2021]. doi:10.1093/g3journal/jkab312
34. Ote M, Ueyama M, Yamamoto D. *Wolbachia* protein TomO targets nanos mRNA and restores germ stem cells in *Drosophila* sex-lethal mutants. Curr Biol. 2016;26: 2223–2232. doi:10.1016/j.cub.2016.06.054
35. Ote M, Yamamoto D. The *Wolbachia* protein TomO interacts with a host RNA to induce polarization defects in *Drosophila* oocytes. Arch Insect Biochem Physiol. 2018;99: e21475. doi:10.1002/arch.21475
36. Li Y, Minor NT, Park JK, McKearin DM, Maines JZ. Bam and Bgcn antagonize Nanos-dependent germ-line stem cell maintenance. Proc Natl Acad Sci. 2009;106: 9304–9309.
37. White PM, Serbus LR, Debec A, Codina A, Bray W, Guichet A, et al. Reliance of *Wolbachia* on high rates of host proteolysis revealed by a genome-wide RNAi screen of *Drosophila* cells. Genetics. 2017; genetics.116.198903. doi:10.1534/genetics.116.198903
38. Li Y, Maines JZ, Tastan OY, McKearin DM, Buszczak M. Mei-P26 regulates the maintenance of ovarian germline stem cells by promoting BMP signaling. Development. 2012;139: 1547–1556. doi:10.1242/dev.077412
39. Neumüller RA, Betschinger J, Fischer A, Bushati N, Poernbacher I, Mechtler K, et al. Mei-P26 regulates microRNAs and cell growth in the Drosophila ovarian stem cell lineage. Nature. 2008;454: 241–245. doi:10.1038/nature07014
40. Page SL, McKim KS, Deneen B, Van Hook TL, Hawley RS. Genetic Studies of *mei-P26* Reveal a Link Between the Processes That Control Germ Cell Proliferation in Both Sexes and Those That Control Meiotic Exchange in Drosophila. Genetics. 2000;155: 1757.
41. Sekelsky JJ, McKim KS, Messina L, French RL, Hurley WD, Arbel T, et al. Identification of novel Drosophila meiotic genes recovered in a P-element screen. Genetics. 1999;152: 529–542.
42. Indrayani Waghmare, Andrea Page-McCaw. Wnt Signaling in Stem Cell Maintenance and Differentiation in the Drosophila Germarium. Genes. 2018;9: 127. doi:10.3390/genes9030127
43. Fast EM, Toomey ME, Panaram K, Desjardins D, Kolaczyk ED, Frydman HM. Wolbachia Enhance Drosophila Stem Cell Proliferation and Target the Germline Stem Cell Niche. Science. 2011;334: 990–992. doi:10.1126/science.1209609
44. Aruna S, Flores HA, Barbash DA. Reduced Fertility of *Drosophila melanogaster Hybrid male rescue* (*Hmr*) Mutant Females Is Partially Complemented by *Hmr* Orthologs From Sibling Species. Genetics. 2009;181: 1437–1450. doi:10.1534/genetics.108.100057
45. Zaccai M, Lipshitz HD. Differential distributions of two adducin-like protein isoforms in the *Drosophila* ovary and early embryo. Zygote. 1996;4: 159–166. doi:10.1017/S096719940000304X
46. Hinnant TD, Merkle JA, Ables ET. Coordinating Proliferation, Polarity, and Cell Fate in the Drosophila Female Germline. Front Cell Dev Biol. 2020;8: 19. doi:10.3389/fcell.2020.00019
47. Zhao R, Xuan Y, Li X, Xi R. Age-related changes of germline stem cell activity, niche signaling activity and egg production in Drosophila. Aging Cell. 2008;7: 344–354. doi:10.1111/j.1474-9726.2008.00379.x
48. Kai T, Spradling A. Differentiating germ cells can revert into functional stem cells in Drosophila melanogaster ovaries. Nature. 2004;428: 564–569. doi:10.1038/nature02436
49. Su TT, Sprenger F, DiGregorio PJ, Campbell SD, O'Farrell PH. Exit from mitosis in *Drosophila* syncytial embryos requires proteolysis and cyclin degradation, and is associated with localized dephosphorylation. Genes Dev. 1998;12: 1495–1503. doi:10.1101/gad.12.10.1495
50. Li Y, Zhang Q, Carreira-Rosario A, Maines JZ, McKearin DM, Buszczak M. Mei-P26 Cooperates with Bam, Bgcn and Sxl to Promote Early Germline Development in the Drosophila Ovary. Singh SR, editor. PLoS ONE. 2013;8: e58301. doi:10.1371/journal.pone.0058301

51. Chau J, Kulnane LS, Salz HK. Sex-lethal Facilitates the Transition From Germline Stem Cell to Committed Daughter Cell in the Drosophila Ovary. Genetics. 2009;182: 121–132. doi:10.1534/genetics.109.100693
52. Tseng C-Y, Kao S-H, Wan C-L, Cho Y, Tung S-Y, Hsu H-J. Notch Signaling Mediates the Age-Associated Decrease in Adhesion of Germline Stem Cells to the Niche. Kim SK, editor. PLoS Genet. 2014;10: e1004888. doi:10.1371/journal.pgen.1004888
53. Chau J, Kulnane LS, Salz HK. Sex-lethal enables germline stem cell differentiation by down-regulating Nanos protein levels during Drosophila oogenesis. Proc Natl Acad Sci. 2012;109: 9465–9470. doi:10.1073/pnas.1120473109
54. Joly W, Chartier A, Rojas-Rios P, Busseau I, Simonelig M. The CCR4 Deadenylase Acts with Nanos and Pumilio in the Fine-Tuning of Mei-P26 Expression to Promote Germline Stem Cell Self-Renewal. Stem Cell Rep. 2013;1: 411–424. doi:10.1016/j.stemcr.2013.09.007
55. Ji S, Li C, Hu L, Liu K, Mei J, Luo Y, et al. Bam-dependent deubiquitinase complex can disrupt germ-line stem cell maintenance by targeting cyclin A. Proc Natl Acad Sci. 2017;114: 6316–6321. doi:10.1073/pnas.1619188114
56. Xie T, Spradling AC. A Niche Maintaining Germ Line Stem Cells in the *Drosophila* Ovary. Science. 2000;290: 328–330. doi:10.1126/science.290.5490.328
57. Chen D, McKearin D. Dpp Signaling Silences bam Transcription Directly to Establish Asymmetric Divisions of Germline Stem Cells. Curr Biol. 2003;13: 1786–1791. doi:10.1016/j.cub.2003.09.033
58. Song X, Wong MD, Kawase E, Xi R, Ding BC, McCarthy JJ, et al. Bmp signals from niche cells directly repress transcription of a differentiation-promoting gene, *bag of marbles* , in germline stem cells in the *Drosophila* ovary. Development. 2004;131: 1353–1364. doi:10.1242/dev.01026
59. Glasscock E. The mei-P26 Gene Encodes a RING Finger B-box Coiled-Coil-NHL Protein That Regulates Seizure Susceptibility in Drosophilia. Genetics. 2005;170: 1677–1689. doi:10.1534/genetics.105.043174
60. Herranz H, Hong X, Pérez L, Ferreira A, Olivieri D, Cohen SM, et al. The miRNA machinery targets Mei-P26 and regulates Myc protein levels in the Drosophila wing. EMBO J. 2010;29: 1688–1698.
61. Ferreira A, Boulan L, Perez L, Milán M. Mei-P26 Mediates Tissue-Specific Responses to the Brat Tumor Suppressor and the dMyc Proto-Oncogene in *Drosophila*. Genetics. 2014;198: 249–258. doi:10.1534/genetics.114.167502
62. Santoso CS, Meehan TL, Peterson JS, Cedano TM, Turlo CV, McCall K. The ABC Transporter *Eato* Promotes Cell Clearance in the *Drosophila melanogaster* Ovary. G3amp58 GenesGenomesGenetics. 2018;8: 833–843. doi:10.1534/g3.117.300427
63. Lantz V, Chang JS, Horabin JI, Bopp D, Schedl P. The Drosophila orb RNA-binding protein is required for the formation of the egg chamber and establishment of polarity. Genes Dev. 1994;8: 598–613.
64. Kaur R, Leigh BA, Ritchie IT, Bordenstein SR. The Cif proteins from Wolbachia prophage WO modify sperm genome integrity to establish cytoplasmic incompatibility. Malik HS, editor. PLOS Biol. 2022;20: e3001584. doi:10.1371/journal.pbio.3001584
65. Turelli M, Hoffmann AA. Cytoplasmic incompatibility in *Drosophila simulans*: dynamics and parameter estimates from natural populations. Genetics. 1995;140: 1319.
66. Yan D, Neumüller RA, Buckner M, Ayers K, Li H, Hu Y, et al. A Regulatory Network of Drosophila Germline Stem Cell Self-Renewal. Dev Cell. 2014;28: 459–473. doi:10.1016/j.devcel.2014.01.020
67. Sheehan KB, Martin M, Lesser CF, Isberg RR, Newton ILG. Identification and characterization of a candidate *Wolbachia pipientis* type IV effector that interacts with the actin cytoskeleton. mBio. 2016;7: e00622-16. doi:10.1128/mBio.00622-16
68. Russell SL, Lemseffer N, White P, Sullivan WT. Wolbachia and host germline components compete for kinesin-mediated transport to the posterior pole of the Drosophila oocyte. McGraw EA, editor. PLOS Pathog. 2018;14: e1007216. doi:10.1371/journal.ppat.1007216
69. Serbus LR, Sullivan W. A cellular basis for *Wolbachia* recruitment to the host germline. PLoS Pathog. 2007;3: e190. doi:10.1371/journal.ppat.0030190
70. Ferree PM, Frydman HM, Li JM, Cao J, Wieschaus E, Sullivan W. *Wolbachia* utilizes host microtubules and dynein for anterior localization in the *Drosophila* oocyte. PLoS Pathog. 2005;1: e14. doi:10.1371/journal.ppat.0010014
71. White PM, Pietri JE, Debec A, Russell SL, Patel B, Sullivan W. Mechanisms of horizontal cell-to-cell transfer of *Wolbachia* spp. in *Drosophila melanogaster*. Appl Environ Microbiol. 2017;83: e03425-16.

doi:10.1128/AEM.03425-16
72. Albertson R, Casper-Lindley C, Cao J, Tram U, Sullivan W. Symmetric and asymmetric mitotic segregation patterns influence *Wolbachia* distribution in host somatic tissue. J Cell Sci. 2009;122: 4570–4583. doi:10.1242/jcs.054981
73. Hackney JF, Pucci C, Naes E, Dobens L. Ras signaling modulates activity of the ecdysone receptor EcR during cell migration in the drosophila ovary. Dev Dyn. 2007;236: 1213–1226. doi:10.1002/dvdy.21140
74. Rastegari E, Kajal K, Tan B-S, Huang F, Chen R-H, Hsieh T-S, et al. WD40 protein Wuho controls germline homeostasis via TRIM-NHL tumor suppressor Mei-p26 in *Drosophila*. Development. 2020;147: dev182063. doi:10.1242/dev.182063
75. Rhiner C, Díaz B, Portela M, Poyatos JF, Fernández-Ruiz I, López-Gay JM, et al. Persistent competition among stem cells and their daughters in the *Drosophila* ovary germline niche. Development. 2009;136: 995–1006. doi:10.1242/dev.033340
76. Chen D, Wu C, Zhao S, Geng Q, Gao Y, Li X, et al. Three RNA Binding Proteins Form a Complex to Promote Differentiation of Germline Stem Cell Lineage in Drosophila. Fuller MT, editor. PLoS Genet. 2014;10: e1004797. doi:10.1371/journal.pgen.1004797
77. Ote M, Yamamoto D. Impact of Wolbachia infection on Drosophila female germline stem cells. Curr Opin Insect Sci. 2020;37: 8–15. doi:10.1016/j.cois.2019.10.001
78. Wang Z, Lin H. Sex-lethal is a target of Bruno-mediated translational repression in promoting the differentiation of stem cell progeny during Drosophila oogenesis. Dev Biol. 2007;302: 160–168. doi:10.1016/j.ydbio.2006.09.016
79. Ye Y, Godzik A. Comparative Analysis of Protein Domain Organization. Genome Res. 2004;14: 343–353. doi:10.1101/gr.1610504
80. Beebe NW, Pagendam D, Trewin BJ, Boomer A, Bradford M, Ford A, et al. Releasing incompatible males drives strong suppression across populations of wild and *Wolbachia* -carrying *Aedes aegypti* in Australia. Proc Natl Acad Sci. 2021;118: e2106828118. doi:10.1073/pnas.2106828118
81. Anderson JA, Gilliland WD, Langley CH. Molecular Population Genetics and Evolution of Drosophila Meiosis Genes. Genetics. 2009;181: 177–185. doi:10.1534/genetics.108.093807
82. Bean DM, Heimbach J, Ficorella L, Micklem G, Oliver SG, Favrin G. esyN: Network Building, Sharing and Publishing. Promponas VJ, editor. PLoS ONE. 2014;9: e106035. doi:10.1371/journal.pone.0106035
83. Casper-Lindley C, Kimura S, Saxton DS, Essaw Y, Simpson I, Tan V, et al. Rapid Fluorescence-Based Screening for Wolbachia Endosymbionts in Drosophila Germ Line and Somatic Tissues. Appl Environ Microbiol. 2011;77: 4788–4794. doi:10.1128/AEM.00215-11
84. Serbus LR, White PM, Silva JP, Rabe A, Teixeira L, Albertson R, et al. The impact of host diet on *Wolbachia* titer in *Drosophila*. PLoS Pathog. 2015;11: e1004777.
85. Bopp D, Bell LR, Cline TW, Schedl P. Developmental distribution of female-specific Sex-lethal proteins in Drosophila melanogaster. Genes Dev. 1991;5: 403–415. doi:10.1101/gad.5.3.403
86. Spradling A. Developmental genetics of oogenesis. Dev Drosoph Melanogaster. 1993.
87. Bolger AM, Lohse M, Usadel B. Trimmomatic: a flexible trimmer for Illumina sequence data. Bioinformatics. 2014;30: 2114–2120. doi:10.1093/bioinformatics/btu170
88. Dobin A, Davis CA, Schlesinger F, Drenkow J, Zaleski C, Jha S, et al. STAR: ultrafast universal RNA-seq aligner. Bioinformatics. 2013;29: 15–21. doi:10.1093/bioinformatics/bts635
89. Li H, Handsaker B, Wysoker A, Fennell T, Ruan J, Homer N, et al. The Sequence Alignment/Map format and SAMtools. Bioinformatics. 2009;25: 2078–2079. doi:10.1093/bioinformatics/btp352
90. Bray NL, Pimentel H, Melsted P, Pachter L. Near-optimal probabilistic RNA-seq quantification. Nat Biotechnol. 2016;34: 525–527. doi:10.1038/nbt.3519
91. Chung M, Bruno VM, Rasko DA, Cuomo CA, Muñoz JF, Livny J, et al. Best practices on the differential expression analysis of multi-species RNA-seq. Genome Biol. 2021;22: 121. doi:10.1186/s13059-021-02337-8
92. Marsh JW, Hayward RJ, Shetty AC, Mahurkar A, Humphrys MS, Myers GSA. Bioinformatic analysis of bacteria and host cell dual RNA-sequencing experiments. Brief Bioinform. 2017 [cited 10 Feb 2023]. doi:10.1093/bib/bbx043
93. Love MI, Huber W, Anders S. Moderated estimation of fold change and dispersion for RNA-seq data with DESeq2. Genome Biol. 2014;15: 550. doi:10.1186/s13059-014-0550-8
94. Soneson C, Love MI, Robinson MD. Differential analyses for RNA-seq: transcript-level estimates improve

gene-level inferences. F1000Research. 2016. doi:10.12688/f1000research.7563.2
95. Li H, Janssens J, De Waegeneer M, Kolluru SS, Davie K, Gardeux V, et al. Fly Cell Atlas: A single-nucleus transcriptomic atlas of the adult fruit fly. Science. 2022;375: eabk2432. doi:10.1126/science.abk2432
96. Ge SX, Jung D, Yao R. ShinyGO: a graphical gene-set enrichment tool for animals and plants. Valencia A, editor. Bioinformatics. 2020;36: 2628–2629. doi:10.1093/bioinformatics/btz931
97. Eklund A. beeswarm. 2023. Available: https://github.com/aroneklund/beeswarm
98. Wickham H. ggplot2: Elegant Graphics for Data Analysis. New York, NY: Springer; 2009. doi:10.1007/978-0-387-98141-3
99. Blighe K, Rana S, Turkes E, Ostendorf B, Grioni A, Lewis M. EnhancedVolcano: Publication-ready volcano plots with enhanced colouring and labeling. Bioconductor version: Release (3.17); 2023. doi:10.18129/B9.bioc.EnhancedVolcano